Heliyon 10 (2024) e28582

Contents lists available at ScienceDirect

Heliyon

journal homepage: www.cell.com/heliyon

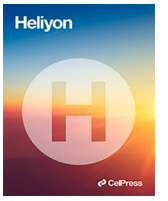

Research article

The anti-depression effect and potential mechanism of the petroleum ether fraction of CDB: Integrated network pharmacology and metabolomics

Jiuseng Zeng [a,1], Li Chen [a,b,1], Xi Peng [a], Fei Luan [c], Jingwen Hu [a], Zhiqiang Xie [a], Hongxiao Xie [a], Rong Liu [a], Haizhen Lv [d], Nan Zeng [a,*]

[a] State Key Laboratory of Southwestern Chinese Medicine Resources, School of Pharmacy, Chengdu University of Traditional Chinese Medicine, Chengdu, 611137, China
[b] Department of Pharmacy, Clinical Medical College and the First Affiliated Hospital of Chengdu Medical College, Chengdu, 610500, China
[c] Shaanxi Key Laboratory of Chinese Medicine Fundamentals and New Drugs Research, School of Pharmacy, Shaanxi University of Chinese Medicine, Xi'an, 712046, China
[d] Department of Pharmacy, Shaanxi Provincial Hospital of Tuberculosis Prevention and Treatment, Xi'an, 710100, China

ARTICLE INFO

Keywords:
Chaidangbo
Petroleum ether fraction
CUMS
Depression
Network pharmacology
Non targeted metabolomics
PI3K/Akt/mTOR signaling pathway

ABSTRACT

The combination of Chaidangbo (CDB) is an antidepressant traditional Chinese medicine (TCM) prescription simplified by Xiaoyaosan (a classic antidepressant TCM prescription) through dismantling research, which has the effect of dispersing stagnated liver qi and nourishing blood in TCM theory. Although the antidepressant effect of CBD has been confirmed in animal studies, the material basis and possible molecular mechanism for antidepressant activity in CBD have not been clearly elucidated. Herein, we investigated the effects and potential mechanisms of CDB antidepressant fraction (petroleum ether fraction of CDB, PEFC) on chronic unpredictable mild stress (CUMS)-induced depression-like behavior in mice using network pharmacology and metabolomics. First, a UPLC-QE/MS was employed to identify the components of PEFC. To extract active ingredients, SwissADME screening was used to the real PEFC components that were found. Potential PEFC antidepressant targets were predicted based on a network pharmacology approach, and a pathway enrichment analysis was performed for the predicted targets. Afterward, a CUMS mouse depression model was established and LC-MS-based untargeted hippocampal metabolomics was performed to identify differential metabolites, and related metabolic pathways. Finally, the protein expressions in mouse hippocampi were determined by Western blot to validate the network pharmacology and metabolomics deduction. A total of 16 active compounds were screened in SwissADME that acted on 73 core targets of depression, including STAT3, MAPKs, and NR3C1; KEGG enrichment analysis showed that PEFC modulated signaling pathways such as PI3K-Akt signaling pathway, endocrine resistance, and MAPK to exert antidepressant effects. PEFC significantly reversed abnormalities of hippocampus metabolites in CUMS mice, mainly affecting the synthesis and metabolism of glycine, serine, and threonine, impacting

* Corresponding author. State Key Laboratory of Southwestern Chinese Medicine Resources, Chengdu University of Traditional Chinese Medicine, Chengdu, 611137, China.
E-mail addresses: zengjiuseng@163.com (J. Zeng), cyfy1219@163.com (L. Chen), pengxi0208@163.com (X. Peng), luanfeiren@163.com (F. Luan), hujingwen@163.com (J. Hu), Xiezhiqiang2408@163.com (Z. Xie), xiehongxiao@stu.cdutcm.edu.cn (H. Xie), liurong_1116@126.com (R. Liu), lhz028@126.com (H. Lv), 19932015@cdutcm.edu.cn (N. Zeng).
[1] These authors have contributed equally to this study.

https://doi.org/10.1016/j.heliyon.2024.e28582
Received 4 November 2022; Received in revised form 15 March 2024; Accepted 20 March 2024
Available online 27 March 2024

catecholamine transfer and cholinergic synapses and regulating the activity of the mTOR signaling pathway. Furthermore, Western blot analysis confirmed that PEFC significantly influenced the main protein levels of the PI3K/Akt/mTOR signaling pathways in the hippocampus of mice subjected to CUMS. This study integrated metabolomics, network pharmacology and biological verification to explore the potential mechanism of PEFC in treating depression, which is related to the regulation of amino acid metabolism dysfunction and the activation of PI3K/Akt/mTOR signaling pathways in the hippocampus. The comprehensive strategy also provided a reasonable way for unveiling the pharmacodynamic mechanisms of multi-components, multi-targets, and multi-pathways in TCM with antidepressant effect.

1. Introduction

Depression, characterized by behavioral despair or anhedonia, is one of the most common psychiatric disorders. It affects an estimated 3.8% of the population globally (https://www.who.int). Current treatments for depression mainly focus on the monoaminergic system, with selective serotonin reuptake inhibitors (SSRIs) being the most clinically used antidepressant [1]. Unfortunately, however, researches have shown that one-third of patients do not respond to initial treatment and frequently experience adverse effects such as nausea, tremors, and insomnia throughout long-term dosing [2]. Thus, it is essential to do additional study and produce antidepressant medications.

Traditional Chinese medicine (TCM), in various forms, has been used for thousands of years to treat depression. Xiaoyaosan is a traditional Chinese remedy that dates to the *Song* Dynasty in China. It is mentioned in the book *Prescriptions of the Bureau of Taiping People's Welfare Pharmacy*. Its benefits include nourishing blood, strengthening the spleen, and distributing sluggish liver *qi* to cure *qi* stasis [3]. The remarkable antidepression effects of Xiaoyaosan against various conditions have been demonstrated extensively [4,5]. Xiaoyaosan exerts its antidepressant effect primarily by inhibiting neuroinflammation, promoting neuroplasticity and synaptic plasticity, and regulating neuroendocrine [6] and amino acid metabolism [7]. Additionally, Xiaoyaosan has been utilized extensively in those who suffer from severe depression, and during which it was shown to possess distinct, its antidepressant effects were clearly demonstrated [4].

The combination of Chaidangbo (CDB), a streamlined formula that exerts antidepressant effects, was created by our research group (*Patent No.: ZL 2014 1 0315781.3*) based on the preliminary exploration of the disassembling prescription and uniform design of Xiaoyaosan [8], CDB, which disperses stagnated liver qi and nourishes blood, consists of three crude herbs, namely *Radix Angelicae Sinensis* (the radix of *Angelica sinensis* (Oliv.) Diels), *Radix Bupleuri* (the radix of *Bupleurum chinense* DC.), and *Herba Menthae Haplocalycis* (the herba of *Mentha haplocalyx* Briq.). In TCM prescriptions, *Radix Bupleuri* is frequently used as a therapeutic herbal medicine to alleviate depression, and it improves symptoms of depression by increasing the serum levels of NGF and BDNF in patients [9]. One study found that the low polarity fraction of *Bupleuri Radix* significantly alleviated depression-like behaviors in the CUMS model rats by improving metabolic profiles and gut microbiota has been reported recently [10]. *Radix Angelicae Sinensis* is a major component of many classical antidepressant TCM prescriptions [11]. Water extracts from *Radix Angelicae Sinensis* have been shown to considerably decrease the duration of immobility in mice in a behavioral despair depression model by improving the contents of monoamine neurotransmitters and neurotrophic factors in the hippocampus [12]. In addition, the active ingredient of *Herba Menthae Haplocalycis* has demonstrated antidepressant-like activity in CUMS-induced depressed mice [13]. More importantly, multiple investigations have established that the aqueous decoction of CDB drastically extenuates depression-like behaviors in the CUMS animal model by upregulating BDNF/TrkB/CREB pathway activity and downregulating HPA axis hyperfunction, with antidepressant effects comparable to those of Xiaoyaosan [14,15].

Pharmacological investigations that use certain extractive fractions extracted from TCM prescriptions as study objectives can efficiently produce novel TCM medications by quickly identifying the primary component groups of base material and adhering to the holistic perspective of TCM philosophy [16]. In our previous research, the antidepressant effect of petroleum ether fraction of CDB (PEFC) has been demonstrated in a mouse model of behavioral despair. However, this antidepressant effect and possible mechanisms are not well defined and must still be evaluated in other models of depression.

The development of memories, storing processes, and emotion regulation are all greatly influenced by the hippocampus, which is also intimately linked to the beginning of depression. Its large concentrations of glucocorticoid receptors and other neurotransmitters are accompanied by its dominating regulation of the HPA axis and impact on neurogenesis, and these characteristics making it more susceptible to stress [17]. Non-targeted metabolomics is a powerful emerging technology for analyzing changes in various metabolites in organisms to offer a complete description of the current metabolic state, providing new perspectives and understanding multifactorial mechanisms of diseases for assessing drug effects from an integrated and holistic perspective [18]. Therefore, for depression, hippocampal metabolomics can yield more critical complementary information in the central nervous system in depression [19]. Non-targeted metabolomics has emerged as a crucial method for figuring out TCM formulations' antidepressant effects in recent years [20]. It is beneficial because it may combine data from the outcomes of interactions between protein function, gene expression, and the cellular environment [21].

With the development of bioinformatics, network pharmacology has gradually become a hot research area. It is based on the principle of systems biology to construct biological networks and elucidate the potential mechanisms of drug therapy for complex diseases [22]. Given that multi-drugs, multi-components, and multi-targets characterize TCM formulas, network pharmacology has

enabled us to effectively link Chinese medicine with its components, targets, pathways, and diseases [23]. The application of network pharmacology provides objective evidence for the intervention of herbal formulas in depression and, more importantly, provides new insight into the development of novel drugs against depression [16,24]. Moreover, an integrated approach that combines network pharmacology and metabolomics is a useful tool for explaining how formulae act as antidepressants. This can result in more comprehensive and accurate predictions of the antidepressant effects of TCM formulas [16,25].

In this study, we first identify the chemical composition of PEFC using UPLC-QE/MS, then apply network pharmacology analysis using bioinformatics tools and systems biology to predict further the genes, proteins, and signaling pathways associated with the antidepressant activity of PEFC [26]. Next, CUMS mouse model was established to assess the antidepressant effects of PEFC, and utilize an LC-MS-based hippocampal untargeted metabolomics approach was applied to validate and expand the potential antidepressant mechanism of action of PEFC. Finally, the partially predicted PEFC antidepressant pathway was validated by the Western blot method. This study evaluates the antidepressant effects of PEFC in a classical CUMS model and reveals possible antidepressant mechanisms that will lay the foundation for developing PEFC as an alternative strategy or drug for the control and treatment of depression.

2. Materials and methods

2.1. Reagents and materials

CDB consisted of three Chinese herbs: the radix of *Bupleurum chinense* DC. *Radix Bupleuri* (Chaihu, batch number: 20180329), the radix of *Angelicae sinensis* (Oliv) Diels. (*Radix Angelicae Sinensis*, Danggui, batch number: 20190618) and the herba of *Menthae haplocalyx* Briq. (*Herba Menthae Haplocalycis*, Bohe, batch number: 181001), all purchased from Tai Chi Pharmacy. (Chengdu, China) and authenticated by Prof. Fei Long, Department of Herbal Resources, Chengdu University of TCM. All plant names were verified on http://www.theplantlist.org. Fluoxetine hydrochloride was acquired from PATHEON FRANCE Co., Ltd (Suzhou, China). Petroleum ether was acquired from Kelong (Chengdu).

2.2. The Preparation of PEFC

Radix Bupleuri, Radix Angelicae Sinensis, and *Herba Menthae Haplocalycis* were mixed in the ratio of 14.4: 14.4: 4.1 as mentioned previously (w/w, with a total weight of 329 g) [15]. The raw herbs were properly crushed together, soaked in 8-fold anhydrous ethanol (v/w) for 12 h, and then subjected to two 2-h extractions, with the resultant decoction concentrated at a lower temperature (45 °C) and pressure (reduced) in a rotary evaporator (Yarong, Zhengzhou, China) to get the crude alcohol extract containing the basic medication.

The alcohol extract was subsequently dispersed in pure water (330 mL) so that the final concentration of the aqueous solution of the alcohol extract was 1 g/mL. The petroleum ether fraction was then obtained by mining the alcohol extract with petroleum ether using a separatory funnel. We first dried the petroleum ether fraction by letting the solvent evaporate in a rotary evaporator before lyophilizing it using a freeze dryer (Songyuan, Beijing, China). Before being employed for analysis, the produced petroleum ether (1.86%) fractions were kept at −20 °C.

2.3. PEFC ingredients identification with UPLC-QE/MS

In the subsequent inquiry, the following chromatographic conditions were used for UPLC-QE/MS analysis of the produced PEFC components: Thermo Scientific AccucoreTM C18 column (2.1 mm × 100 mm, 2.2 μm), mobile phase water + 0.1% formic acid (aqueous phase, AP), acetonitrile (organic phase, OP), gradient elution (0–5 min, 10% ~ 40% OP; 5–30 min, 40%–55% OP; 30–38 min, 55%–60% OP; 38–50 min, 60%–90% OP; 50–55 min, 90% OP), a column temperature of 30 °C, an injection volume of 5.0 μL, and a flow rate of 0.3 mL/min. The following characteristics were chosen: spray voltage of 3000 V, 350 °C for the ion source, 35 arb for the sheath gas flow rate, 10 arb for the auxiliary gas flow rate, and 320 °C for the ion transfer tube temperature. Mass spectrometric conditions were also used. With a scan range of m/z 100 to 1500, an instantaneous resolution of 70 000, and a secondary resolution of 17 500, a complete scan/data-dependent secondary scan was employed as the scanning mode.

In order to coordinate with the possible molecular formulae, the resulting molecular ion chromatogram peaks and isotope peaks were extracted, and the measured secondary fragment spectra matched with the mzCloud online database. The collected raw data were imported into Compound Discoverer 3.0 (Thermo Scientific, USA) for peak alignment and peak extraction. In order to identify compounds analytically, ions with a matching degree score greater than 80 were chosen and further aligned with the compound information in the relevant literature and databases. Fig. S1 in the Supplementary Material displays the UPLC-QE/MS total ion flow chromatogram of PEFC. Ligustilide (the most abundant compound in PEFC) was subsequently scrutinized quantitatively with HPLC for quality control details in Supplementary Material, Fig. S2.

2.4. Network pharmacology analysis

2.4.1. Identification of PEFC ingredient-related targets

The main chemical components of PEFC were screened using the SwissADME database (http://www.swissadme.ch/) [27]. Chemical components that met the GI absorption parameter “high” and the BBB permeation parameter “yes” with relative abundance higher than 0.1% and satisfied the five principles of Lipinski drug-likeness properties were selected as the main components for the pharmacological action of PEFC.

The SwissTargetPrediction database (http://www. swisstargetprediction.ch/) was used to predict the targets of the active compounds. The 2D structural SDF format (.sdf) of these candidate active ingredients of PEFC were downloaded from the PubChem database and submitted to SwissTargetPrediction [28]. Species were selected as "*Homo sapiens*", and targets with a probability higher than 0 were chosen for identification as potential targets.

2.4.2. Disease-associated target collection

The currently known potential therapeutic targets for depression were gathered from the OMIM database (http://www.omim.org), TTD database (http://db.idrblab.net/ttd/), PharmGKB database (https://www.pharmgkb.org/), NCBI database (https://www.ncbi.nlm.nih.gov/) and GeneCards database (http://www.genecards.org/) using the keywords "depression" and "antidepression". All targets enrolled in this research were human genes/proteins.

2.4.3. Network construction and topological analysis

Targets that overlapped between depression and active substances were found and added to the STRING database (https://www.string-db.org/); the species was set as "*Homo sapiens*", and the interaction results were saved in TSV format (.tsv). The CytoNCA Tool in Cytoscape was utilized to do further analysis on the nodes' degree, closeness centrality, and betweenness centrality, which signify their topological significance in the network [29]. Nodes with a degree, closeness centrality, and betweenness centrality above averages were defined as core targets. The core targets were introduced into Cytoscape 3.6.0 to construct and visualize protein-protein interaction (PPI) and "component-core target" composite networks.

2.4.4. GO and KEGG enrichment analyses

Gene Ontology (GO) and Kyoto Encyclopedia of Genes and Genomes (KEGG) were used to examine biological processes, cellular components, molecular functions, and signaling pathways associated with depression and modulated by PEFC [25]. The core targets of PEFC antidepressant effects were imported into the DAVID database (https://david.ncifcrf.gov/), and the identification and species selected for GO and KEGG enrichment analysis were "OFFICIAL_GENE_SYMBOL" and "*Homo sapiens*", respectively [30]. GO terms and KEGG pathways with a *p-value*<0.05 were considered statistically significant. The most substantial entries were chosen for visualization using the R software, and histograms for GO analyses and bubble plots for KEGG analysis were drawn.

2.5. Animal experiment

2.5.1. Animals

Male C57BL/6J mice aged five weeks were purchased from SPF Biotechnology Co., Ltd. in Beijing, China; qualify code: SCXK-[Jing]-2019-0010) were grown in typical cages in a room with a 12:12 light/dark cycle, consistent humidity and temperature (50–75%; 22 ± 2 °C). The Chengdu University of Traditional Chinese Medicine College of Pharmacy's Committee for Animal Care and Use of Laboratory Animals approved the experimental procedures; TCM-2019-312 was the approval number for this process.

2.5.2. CUMS model protocol and treatment

The CUMS procedure is the standard paradigm in depression research because it replicates people's ongoing annoyance in reaction to uncontrollably negative social experiences [31]. The CUMS model was performed as in our previous report [3]. In brief, C57BL/6J mice in the CUMS groups were subjected to a variety of stressors following a week of adaption, including wet pad (12 h), physical restraint (3 h), food deprivation (12 h), water deprivation (12 h), swimming in ice water (4 °C, 4 min), tail clip (3 min), noise (1 h), absence of bedding (12 h), crowding (12 h), thermal stimulation (45 °C, 5 min), vinegar stimulation (3 h), overnight illumination (12 h), a 45°cage tilt (12 h), and cage shaking (10 min) for consecutive eight weeks. Every day, two distinct stressors were administered, and every seven days, the order of stressors was switched. C57BL/6J mice that were not under stress were housed in unaltered cages. The schematic of the experimental procedure is shown in Fig. 1.

The sucrose preference test (SPT) was used to determine if the CUMS model had been successfully created after four weeks of the CUMS method. Mice displaying anhedonia behavior, which is a primary CUMS symptom, were divided into 5 groups at random (n = 10 per group): groups CUMS and CUMS + FLX (fluoxetine, 13.2 mg kg^{-1}, i.g.) [3] group, CUMS + PEFC group (0.205 g kg^{-1}, 0.409 g kg^{-1}, 0.818 g kg^{-1}, i.g., corresponding to herbs 11.0 g kg^{-1}, 22.0 g kg^{-1} and 44.0 g kg^{-1}) group. The behavioral despair depression model

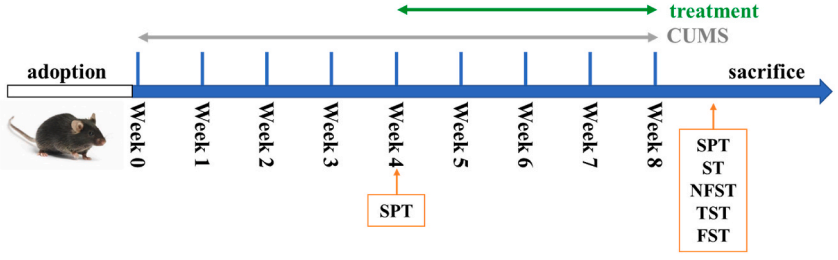

Fig. 1. Schematic diagram of the experimental animal study process.

experiment findings were used to determine the PEFC dosages for CUMS therapy (Supplementary Material, Fig. S4). PEFC or FLX was administered intragastrically, once daily, from 10:00 a.m. to 11:30 a.m. from weeks 5–8, with chronic treatment modalities and CUMS stimulation continuing throughout the treatment period. 0.5% carboxymethyl cellulose Na (CMC Na) and 0.5% TWEEN 80 solution were used to dissolve PEFC and FLX, whereas an equivalent volume of solvent was provided to the control group.

Mice were given sodium pentobarbital anesthesia 12 h after behavioral testing, and blood was drawn from their retro-orbital plexus. The blood was then centrifuged at a low speed (3000 r/min for 15 min) in order to separate the serum. After dissecting hippocampal tissues on ice, samples were quickly frozen in liquid nitrogen and kept as a backup at −80 °C.

2.5.3. Behavioral tests

Testing on behavior began at the conclusion of the eighth week. To minimize interference between behavioral tests, we conducted only one behavioral test each day in the following sequence: sucrose preference test (SPT), splash test (ST), novelty-suppressed feeding test (NSFT), tail suspension test (TST) and forced swimming test (FST). To avoid evaluating the full group at once, all of the tests were carried out in parallel on all of the mice [32]. In addition, all behavioral tests were conducted in low light and noise levels with blind guidance on drug administration.

Sucrose preference test (SPT): The SPT was utilized to evaluate the level of anhedonia in mice, which is a fundamental sign of depression. To ensure that the experiment was not impacted by the eating habits of the animals, two water bottles were positioned in each cage. Prior to the experiment, every mouse underwent a 24-h water fast. On the day of the test, the home cage was left with 3 h of drinking water and a 1% sucrose solution. And sucrose preference was calculated using the following equation: sucrose preference (%) = sucrose intake/(sucrose intake + water intake) × 100% [33].

Splash test (ST): The Self-Test measures self-motivation and self-care, and its results are assumed to mirror some depressive symptoms, such apathy. Standard mouse cages without any bedding were used for the ST procedures. To encourage grooming activity, we sprayed mice's dorsal ends with a 2 mL 10% sucrose solution in their home cages. We then timed how long the mice spent grooming over the course of 5 min [34].

Novelty-suppressed feeding test (NFST): The NSFT evaluates a mouse's reaction to incentives and perceptions of its environment. The mice were placed in an open field (40 × 40 × 20 cm) with a modest amount of food placed at the center after being fasted for 36 h and allowed to acclimate to the experimental setting for an additional hour. The feeding latency was measured by timing how long it took the mice to bite into the meal; they had up to 5 min [35].

Tail suspension test (TST): The animal's behavioral desperation and lack of escape-related activity are represented by the immobility time in the TST. For a duration of 6 min, mice were hung with a tape approximately 1.5 cm from the tail tap and more than 35 cm above the floor. During this time, two observers recorded each mouse's immobility time for analysis during the last 4 min of the test [36].

Forced swimming test (FST): Another crucial test for observing animals' despairing behavior is the FST [37]. Each mouse in FST was put in a plastic bucket that was 12 cm in diameter and 25 cm deep in water (22–24 °C). The FST lasted 6 min, with the final 4 min of the test being spent immobile for two observers to analyze the data.

2.5.4. Enzyme-linked immunosorbent assay

According to the manufacturer's instructions, the serum levels of Cort were measured using an ELISA kit (Lot No. E-EL-0161c, Elabscience Technology Co. Ltd., Wuhan, China). In short, a 96-well plate pre-coated with target antibody received 50 μL of frozen standards and serum samples, and then 100 μL of horseradish peroxidase-conjugated antibody was added. Following a 60-min incubation period at 37 °C, the liquid was disposed of. Following that, 350 μL of washing buffer was used to wash each well five times. Each well was then filled with 50 μL of substrate A and B, and the wells were left to incubate for 15 min in the dark at 37 °C. Following the addition of 50 μL of termination solution to each well, a microplate reader was used to measure the absorbance at 450 nm. The standard curve was used to determine the serum Cort levels.

2.5.5. LC-MS hippocampus metabolomics analysis

The experiment was performed on four random hippocampal samples of approximately 15 mg from each group size. 100 μL of the 2-LV phenylalanine (4 ppm) extractant configured with methanol was added to the samples, the mixture was centrifuged directly, and the supernatant was collected for testing.

Chromatographic separation was accomplished in a Thermo Vanquish system equipped with an ACQUITY UPLC HSS T3 column (150 × 2.1 mm, 1.8 μm) maintained at 40 °C. The autosampler's temperature was 8 °C. Using 0.1% formic acid in water (A1), 0.1% formic acid in acetonitrile (B1), or 5 mM ammonium formate in water (A2) and acetonitrile (B2) at a flow rate of 0.25 mL/min, gradient elution of analytes was performed. Once equilibrated, 2 μL of each sample was injected. An increasing linear gradient of solvent B1/B2 (v/v) was used as follows: 0–1 min, 2% B1/B2; 1–9 min, 2%–50% B1/B2; 9–12 min, 50%–98% B1/B2; 12~13.5 min, 98% B1/B2; 13.5–14 min, 98%–2% B1/B2; 14–20 min, 2% B1-positive model (14–17 min, 2% B3-negative model).

Thermo Q Exactive mass spectrometer was used for ESI-MSn studies, with spray voltages set to 3.5 kV in the positive mode and −2.5 kV in the negative mode, respectively. The auxiliary gases and the sheath were adjusted to 30 and 10 arbitrary units, respectively. 325 °C was the capillary temperature. For a complete scan at a mass resolution of 70 000, the analyzer covered a mass range of m/z 81-1000. An HCD scan was used for data dependent acquisition (DDA) MS/MS investigations. The normalized collision energy was 30 eV. Some unnecessary information in the MS/MS spectra was removed using dynamic exclusion.

Table 1
The main chemical components of PEFC.

No.	tR/ min	Component name	Relative content (%)	Mw	ppm	PubChem CID	Molecular formula	Mode	MS/MS
C1	0.757	DL-Arginine	0.1900	174.2	−0.71	232	$C_6H_{14}N_4O_2$	Pos (+)	175.12[M+H]+
C2	0.791	Choline	0.0750	104.17	1.6	305	$C_5H_{14}NO$+	Pos (+)	104.11[M]+
C3	0.82	D-(+)-Maltose	0.0410	342.3	−0.99	439186	$C_{12}H_{22}O_{11}$	Neg (−)	341.11[M − H]-; 313.11 [M-H-CO]-
C4	0.827	α,α-Trehalose	0.3960	342.12	−0.23	3231	$C_{12}H_{22}O_{11}$	Neg (−)	341.11[M − H]-; 313.11 [M-H-CO]-
C5	0.828	α-Lactose	0.0250	359.14	1.91	242081360	$C_{12}H_{22}O_{11}$	Pos (+)	360.15[M+H]+; 381.18 [M + Na–H]+
C6	0.834	D-(+)-Arabitol	0.0190	152.15	−3.9	94154	$C_5H_{12}O_5$	Neg (−)	151.06[M − H]-; 134.86 [M − H_2O]-
C7	0.855	4-Guanidinobutyric acid	0.0130	145.16	0.13	500	$C_5H_{11}N3O_2$	Neg (−)	144.99[M − H]-; 127.41 [M − H_2O]-
C8	4.181	Vanillin	0.0470	152.15	0.03	1183	$C_8H_8O_3$	Neg (−)	151.04[M − H]-; 136.02 [M − NH_2]-
C9	4.383	Ferulic acid	0.1420	194.18	−0.01	445858	$C_{10}H_{10}O_4$	Pos (+)	195.07[M+H]+; 177.05 [M + H–H_2O]+; 154.99 [M + H–Na]+
C10	5.555	Geranic acid	0.0340	168.12	0.53	5275520	$C_{10}H_{16}O2$	Pos (+)	169.98[M+H]+; 196.02 [M + CO]+
C11	6.078	Quercetin	0.0170	302.23	0.72	5280343	$C_{15}H_{10}O_7$	Pos (+)	303.05[M+H]+; 327.01 [M+2H+2Na]+
C12	6.139	10-Hydroxy-2-decenoic acid	0.0290	186.25	1.35	5312738	$C_{10}H_{18}O_3$	Neg (−)	187.86[M+H]-; 168.89 [M − H_2O]-
C13	6.478	Ethyl caffeate	0.0100	208.21	−0.82	5317238	$C_{11}H_{12}O_4$	Neg (−)	207.07[M − H]-; 189.90 [M-NA + H]-
C14	6.948	Saikosaponin C	0.0440	972.53	0.86	131801344	$C_{48}H_{78}O_{18}$	Neg (−)	971.52[M − H]-; 649.37 [M-Glc-Fuc+3H]-
C15	7.081	Diosmetin	0.0230	300.26	0.32	5281612	$C_{16}H_{12}O_6$	Neg (−)	299.06[M − H]-;
C16	7.24	3-Methoxy-5,7,3′,4′-tetrahydroxy-flavone	0.0300	316.06	0.28	ND	$C_{16}H_{12}O_7$	Pos (+)	317.07[M+H]+; 348.27 [M+2O]+
C17	7.435	(15*Z*)-9,12,13-Trihydroxy-15-octadecenoic acid	0.0390	330.5	0.06	24066906	$C_{18}H_{34}O_5$	Neg (−)	329.23[M − H]-; 329.23 [M-H + CO]-
C18	7.557	Methoxsalen	0.0300	216.19	0.54	4114	$C_{12}H_8O_4$	Pos (+)	217.05[M+H]+; 279.16 [M+2Na + H_2O]+
C19	7.982	Oleanonic acid	0.0250	454.7	−1.01	12313704	$C_{30}H_{46}O_3$	Pos (+)	455.35[M+H]+; 484.31 [M+2H + CO]+
C20	8.07	6-Pentyl-2H-pyran-2-one	0.0480	166.22	−0.1	33960	$C_{10}H_{14}O_2$	Pos (+)	167.11[M+H]+; 182.99 [M + NH_2]+
C21	8.333	Ethyl ferulate	0.0040	222.24	0.32	736681	$C_{12}H_{14}O_4$	Pos (+)	221.08[M − H]-; 195.81 [M − CO]-
C22	8.592	Isophorone	0.0620	138.21	0.49	6544	$C_9H_{14}O$	Pos (+)	139.11[M+H]+
C23	8.761	Carvone	0.8030	150.22	0.67	7439	$C_{10}H_{14}O$	Pos (+)	151.11[M+H]+; 169.98 [M + H + H_2O]+
C24	9.08	Scoparone	0.3850	206.19	−0.23	8417	$C_{11}H_{10}O_4$	Pos (+)	207.07[M+H]+
C25	9.121	Saikosaponin A	0.5930	781	0.01	167928	$C_{42}H_{68}O_{13}$	Pos (+)	781.41[M+H]+; 763.46 [M + H + H2O]+; 455.35 [M-Glc-Fuc]+
C26	9.14	4-hydroxy-3-(3-methylbut-2-enyl) benzoic acid	0.0500	206.24	−1.13	443852	$C_{12}H_{14}O_3$	Pos (+)	207.07[M+H]+; 274.27 [M + C5H6]+
C27	10.585	β-Elemonic acid	0.0330	454.34	−0.97	348290102	$C_{30}H_{46}O_3$	Pos (+)	455.35[M+H]+; 437.34 [M + H–H2O]+; 459.72 [M+Na]+
C28	10.917	Skullcapflavone II	0.0710	374.3	0.13	124211	$C_{19}H_{18}O_8$	Pos (+)	375.11[M+H]+;
C29	11.007	Wogonin	0.0190	284.26	0.02	5281703	$C_{16}H_{12}O_5$	Pos (+)	285.08[M+H]+; 331.04 [M+3H + CO2]+
C30	11.012	Methyl cinnamate	0.1990	162.18	−0.26	637520	$C_{10}H_{10}O_2$	Pos (+)	163.08[M+H]+; 131.05 [M + CO–H_2O]+
C31	11.344	Jasmone	0.0120	164.24	0.42	1549018	$C_{11}H_{16}O$	Pos (+)	165.13[M+H]+; 182.99 [M + H + H_2O]+; 189.09 [M + H + Na]+

(*continued on next page*)

Table 1 (*continued*)

No.	tR/ min	Component name	Relative content (%)	Mw	ppm	PubChem CID	Molecular formula	Mode	MS/MS
C32	11.871	Kurarinone	0.0080	438.5	0.42	11982640	$C_{26}H_{30}O_6$	Pos (+)	439.36[M+H]+; 421.35 [M + H–H_2O]+
C33	12.073	9*S*,13*R*-12-Oxophytodienoic acid	0.0200	292.4	−0.14	14037063	$C_{18}H_{28}O_3$	Pos (+)	393.21[M+H]+; 316.28 [M + H + Na]+
C34	12.766	Senkyunolide A	0.8640	192.25	0.71	3085257	$C_{12}H_{16}O_2$	Pos (+)	193.12 [M+H]+
C35	13.082	α-Pinene-2-oxide	0.2690	152.12	−0.39	387130156	$C_{10}H_{16}O$	Pos (+)	154.99 [M+2H]+; 169.98[M + H_2O]+
C36	15.187	2-Aminooctadec-4-yne-1,3-diol	0.0120	297.5	0.12	2802958	$C_{18}H_{35}NO_2$	Pos (+)	298.27[M+H]+; 316.28 [M + H + H_2O]+; 327.01 [M+2H + CO]+
C37	15.447	2-Amino-1,3,4-octadecanetriol	0.0400	317.5	−0.46	248575	$C_{18}H_{39}NO_3$	Pos (+)	318.30[M+H]+; 389.12 [M + $C_4H_{10}N$]+
C38	15.562	3-*n*-Butylphathlide	10.0130	190.24	0.2	61361	$C_{12}H_{14}O_2$	Pos (+)	191.11[M+H]+; 173.10 [M + H–H_2O]+
C39	16.448	4-methyl-6-phenyl-5,6-dihydro-2H-pyran-2-one	0.3720	188.22	0.15	2817525	$C_{12}H_{12}O_2$	Pos (+)	189.09[M+H]+
C40	16.673	α-Linolenic acid	0.0190	278.22	−0.6	184021992	$C_{18}H_{30}O_2$	Pos (+)	279.23[M+H]+; 280.24 [M+2H]+
C41	16.753	Sedanolide	0.0560	194.27	0.52	5018391	$C_{12}H_{18}O_2$	Pos (+)	195.14[M+H]+; 415.21 [2 M + Na]+
C42	17.399	Ligustilide	62.6400	190.24	0.2	5319022	$C_{12}H_{14}O_2$	Pos (+)	191.11[M+H]+; 173.10 [M + H–H_2O]+
C43	17.502	Isoeugenol acetate	0.0610	206.24	1.63	876160	$C_{12}H_{14}O_3$	Neg (−)	205.55[M − H]-; 197.81 [M − H_2O]-;
C44	17.967	(±)9-HpODE	0.0410	312.4	0.85	6439847	$C_{18}H_{32}O_4$	Neg (−)	311.22[M − H]-; 245.89 [M − C_5H_7]-
C45	18.071	3-Butylidenephthalide	0.5020	188.22	−0.71	642376	$C_{12}H_{12}O_2$	Pos (+)	191.11 [M+3H]+; 207.10[M + H_2O]+
C46	18.558	Bis(4-ethylbenzylidene)sorbitol	0.0300	414.2	−0.46	387149854	$C_{24}H_{30}O_6$	Pos (+)	415.21[M+H]+; 455.35 [M + Na + H_2O]+
C47	18.612	Dehydrotrametenolic acid	0.0190	454.7	−0.88	15391340	$C_{30}H_{46}O_3$	Pos (+)	455.35[M+H]+; 519.20 [M + C_5H_6]+
C48	19.519	Gardenin B	0.2370	358.11	−0.28	96539	$C_{19}H_{18}O_7$	Pos (+)	359.11[M+H]+
C49	20.955	9-(acetyloxy)-8,8-dimethyl-2-oxo-9,10-dihydro-2H,8H-pyrano [2,3-f]chromen-10-yl 2-methyl-2-butenoate	0.5420	386.4	−0.51	5316002	$C_{21}H_{22}O_7$	Pos (+)	287.09[M-$C_5H_8O_2$+H]; 404.17[M + H_2O]+
C50	21.447	Methyl palmitate	0.0180	270.5	0.23	8181	$C_{17}H_{34}O_2$	Pos (+)	271.26[M+H]+; 287.09 [M + H_2O–H]+
C51	21.683	10-(acetyloxy)-8,8-dimethyl-2-oxo-2H,8H,9H,10H-pyrano[2,3-h] chromen-9-yl (2*Z*)-2-methylbut-2-enoate	0.0430	403.16	0.21	9821539	$C_{21}H_{22}O_7$	Pos (+)	404.17[M+H]+; 432.2 [M + H + CO]+
C52	23.155	Senkyunolide H	0.1830	224.25	−0.83	13965088	$C_{12}H_{16}O_4$	Pos (+)	207.10[M+H]+; 230.14 [M + H + Na]+; 189.09 [M-H2O]+
C53	23.559	2-Methoxy-9H-xanthen-9-one	0.0130	226.23	−0.22	71034	$C_{14}H_{10}O_3$	Pos (+)	227.07[M+H]+; 245.08 [M + H + H_2O]+
C54	24.956	9-(Acetyloxy)-8,8-dimethyl-2-oxo-9,10-dihydro-2H,8H-pyrano [2,3-f]chromen-10-yl 2-methyl-2-butenoate	0.1130	386.4	1.56	5316002	$C_{21}H_{22}O_7$	Pos (+)	404.17[M + NH_4]+
C55	25.276	12-Oxo phytodienoic acid	0.0260	292.4	0.24	188366	$C_{18}H_{28}O_3$	Pos (+)	293.21[M+H]+; 309.21 [M + NH_3+]+; 315.19 [M+Na]+
C56	27.087	3-Methoxycinnamic acid	0.0200	178.18	−1.39	637668	$C_{10}H_{10}O_3$	Pos (+)	179.19[M+H]+
C57	31.094	9-Oxo-10,12-octadecadienoic acid	0.6390	294.41	−0.25	5283011	$C_{18}H_{30}O_3$	Neg (−)	293.21[M − H]-; 245.89 [M-4H–CO_2]-
C58	32.205	(9cis)-Retinal	0.0440	284.21	−0.47	6436082	$C_{20}H_{28}O$	Pos (+)	285.22[M+H]+;
C59	35.279	Levistilide A	9.3770	380.5	−0.65	70698035	$C_{24}H_{28}O_4$	Pos (+)	381.21 [M+H]+; 398.23 [M + H_2O]+; 403.19 [M+Na]+

(*continued on next page*)

Table 1 (*continued*)

No.	tR/ min	Component name	Relative content (%)	Mw	ppm	PubChem CID	Molecular formula	Mode	MS/MS
C60	42.038	Methyl alpha-eleostearate	0.0160	292.24	−0.03	21718552	$C_{19}H_{32}O_2$	Pos (+)	293.25[M+H]+; 338.34 [M+2H + CO_2]+
C61	44.365	1-Linoleoyl glycerol	0.0790	354.5	−0.23	117319	C21H38O4	Neg (−)	279.16[M-$C_3H_7O_2$]-; 261.29 [M–$C_3H_7O_2$–H_2O]-
C62	44.674	16-Hydroxyhexadecanoic acid	0.7740	272.42	0.47	10466	$C_{16}H_{32}O_3$	Neg (−)	271.23[M − H]-; 243.90 [M–CO–H]-
C63	44.701	α-Eleostearic acid	0.5530	278.22	0.08	7850014	$C_{18}H_{30}O_2$	Pos (+)	279.23[M+H]+; 338.34 [M+3Na]+
C64	45.003	Oleanolic acid	0.5600	456.7	0.71	10494	$C_{30}H_{48}O_3$	Neg (−)	455.35[M − H]-; 271.23 [M-$C_{15}H_{28}$+Na]-
C65	45.182	γ-Linolenic acid ethyl ester	0.0150	306.26	−0.34	445551954	$C_{20}H_{34}O_2$	Pos (+)	307.26[M+H]+; 325.22 [M + H + H_2O]+
C66	47.037	Oleamide	0.5550	281.5	−0.65	5283387	$C_{18}H_{35}NO$	Pos (+)	282.28[M+H]+; 327.23 [M+2Na]+
C67	48.02	Dibutyl sebacate	0.0100	314.5	0.11	7986	$C_{18}H_{34}O_4$	Pos (+)	315.25[M+H]+; 339.16 [M+2H + Na]+
C68	48.293	Lupenone	0.0190	424.7	−0.36	92158	$C_{30}H_{48}O$	Pos (+)	425.38[M+H]+; 482.46 [M + H + C_4H_8]+
C69	48.551	Isoreserpin	0.0770	608.7	−0.58	5052	$C_{33}H_{40}N_2O_9$	Pos (+)	609.27[M+H]+; 634.45 [M+3H + Na]+
C70	50.618	Palmitic acid	0.0170	256.24	0.28	985	$C_{16}H_{32}O_2$	Neg (−)	255.23[M − H]-; 208.07 [M-2H–2Na]-
C71	51.095	Elaidic acid	0.0270	282.5	0.31	637517	$C_{18}H_{34}O_2$	Pos (+)	283.26[M+H]+; 326.34 [M + CO_2]+
C72	51.787	Stearamide	1.0140	283.5	−0.85	31292	$C_{18}H_{37}NO$	Pos (+)	284.29[M+H]+; 312.33 [M + CO + H]+
C73	52.314	1-Stearoylglycerol	0.0190	358.31	−0.71	22035687	$C_{21}H_{42}O_4$	Pos (+)	437.19[M + H + C_6H_6]+

2.5.6. Western blot analysis

To assess the total protein content, 1 mM phosphatase inhibitor cocktail and 1 mM PMSF were added to each sample in a RIPA lysate buffer. Using the BCA test technique, the total protein concentration of each sample was measured, and each sample's concentration was corrected to match. Samples of protein were combined with a loading buffer of 5 × , denatured at 95 °C, separated by sodium dodecyl sulfate-polyacrylamide gel electrophoresis (SDS-PAGE), and then electrophoretically transferred onto membranes made of polyvinylidene fluoride. These membranes were probed with rabbit anti-p-PI3 Kinase (1:1000; CST®; #17366S), rabbit anti-PI3 Kinase (1:1000; CST®; Cat. No. #4249T), rabbit anti-*p*-Akt (1:1000; CST®; #4060S), rabbit anti-Akt (1:1000; CST®; #4691S), rabbit anti-*p*-mTOR (1:1000; CST®; #2983S), rabbit anti-mTOR (1:1000; CST®; #5536S), rabbit anti-GR (1:1000; CST®; #12041S) and rabbit anti-β actin (1:1000; Servicebio®; #GB113225) antibodies overnight at 4 °C, anti-rabbit IgG HRP-conjugated antibody (1:3000; Servicebio®; #GB23303) was added the next day at indoor temperature for 80 min. A Chemi-Doc XRS + image analysis system (BioRad, USA) was used to measure total protein.

2.6. Statistical analysis

LC-MS raw data were processed using the Proteowizard software (v3.0.8789). A mass-to-nucleus ratio (*m/z*) data mapping was performed, and retention time and peak area (intensity) information were obtained. The data were exported to Microsoft Excel for principal component analysis (PCA) and orthogonal partial least squares discriminant analysis (OPLS-DA) using the online tool Biodeep cloud platform (http://www.biodeep.cn/home). The online tool was also used to help identify metabolite differences and construct metabolic pathways. The means ± standard deviations were used to represent all data, including those from the biochemical analysis and behavioral testing. Using SPSS 21 (IBM, Armonk, NY, USA), the one-way analysis of variance was utilized for all analyses (for pairwise comparisons between groups, SNK was utilized). Differences were considered statistically significant at $P < 0.05$.

3. Results

3.1. Compound identification of PEFC and active component screening

Peak area normalization was utilized to ascertain the respective component's percentage. The exact chemical makeup of the discovered PEFC is displayed in Table 1. Seventy-two compounds were found in all, making up 93.47% of the area of all the peaks in PEFC that were discovered. Among these compounds, Ligustilide (C42), 3-*n*-butylphthalide (C38), Levistilide A (C59) were originated from *Angelica sinensis* with 62.640%, 10.013%, 9.377% in PEFC, respectively; Carvone (C23) from *Herba Menthae* and Saikosaponin A (C25) from *Radix Bupleuri* with 0.803% and 0.593% in PEFC, respectively. The five compounds mentioned above make up the main

component, accounting for nearly 80% of all peak areas. Next, we extracted compounds with relative content greater than 0.1% as the main components of PEFC. Sixteen active compounds were screened in the SwissADME database according to specific parameters, including GI absorption, BBB penetration, and drug-likeness (Table 2.).

3.2. Target and network analysis of PEFC for depression

The SMILES of the 16 abovementioned active compounds were plotted in the SwissTargetPrediction database to each compound's potential targets, establishing 372 compound-related targets after removing duplicates (Supplementary Material, Table S1). Additionally, five databases (PharmGKB, GeneCards, OMIM, NCBI, and TTD) produced 2314 targets for depression after screening (Supplementary Material, Table S2). Analyses showed that the 372 compound-related targets matched the 2314 disease-related targets, yielding 152 overlapping targets (Fig. 2A; Supplementary Material, Table S3). Subsequently, the 152 overlapping targets were imported into STRING, and the TSV format files of the interaction results were analyzed using the CytoNCA tool in Cytoscape. 73 nodes with a degree, closeness centrality, and betweenness centrality above the median were screened as the core targets of PEFC antidepressants. The compound-target network of PEFC for depression was developed and presented using Cytoscape with the addition of 73 overlapped genes and 16 active compounds. 89 nodes and 147 edges made up this network (Fig. 2B). The core antidepressant targets of PEFC were introduced into STRING and visualized using Cytoscape PPI network maps for further analysis. In the PPI network diagram, darker the color and larger the area of the node, greater the "degree" and the higher relevance of its involvement in the antidepressant effect of PEFC. Genes such as *STAT3*, *MAPK1/3*, *PIK3CA*, *ESR1*, *MAPK8/14*, *NR3C1*, and *JAK2* could be potential research targets for PEFC in treating depression (Fig. 2C).

3.3. GO and KEGG enrichment analyses of the antidepressant effect of PEFC

GO enrichment analyses were performed on the 73 overlapping targets to predict the gene/protein functions and signaling pathways of PEFC involved in the treatment of depression further (Supplementary Material, Table S4). The GO biological process (BP), cellular component (CC), and molecular function (MF) top 20 items are ranked by *p-value*, as seen in Fig. 3A, which showed that these potential targets are mainly located in cellular components like receptor complexes, axons, glutamatergic synapses, and neuronal cell body; regulating molecular functions like protein binding, enzyme binding, ATP binding, and protein kinase binding; and affecting biological processes such as protein phosphorylation, kinase activity, cell migration, and MAPK/protein kinase B signaling cascade. Per KEGG analysis, the 73 overlapping genes in which PEFC exerts antidepressant effects were significantly enriched in multiple signaling pathways ($P < 0.05$, Supplementary Material, Table S5). The top 30 pathways were selected for bubble map visualization (Fig. 3B), where the PI3K-Akt pathway, endocrine resistance, pathways of neurodegeneration, and the MAPK signaling pathway exhibited a high degree of enrichment.

3.4. Treatment with PEFC reversed CUMS-induced depression-like behaviors

After four weeks of CUMS stimuli, all CUMS mice had a substantial drop in their sucrose preference rate ($P < 0.05$; Fig. 4A), suggesting that the model mice had a malfunctioning brain reward mechanism, a central symptom of depression. According to these findings, the CUMS model was effectively replicated by week four, when medication delivery to the treatment groups started in addition to ongoing CUMS stimulation.

Treatment with PEFC (22.0 g kg^{-1}, 44.0 g kg^{-1}, $P < 0.05$) and FLX ($P < 0.05$) for 4 weeks markedly reversed the CUMS-induced reduction in the percentage of sucrose preference (Fig. 4B). Further behavioral testing was done to ascertain the antidepressant impact of PEFC, including the ST, NFST, TST, and FST. In the ST, combing time reduced considerably in the CUMS group animals compared to

Table 2
Components of PEFC after SwissADME database screening.

No.	Component	Relative content (%)	Formula
C42	Ligustilide	62.64	$C_{12}H_{14}O_2$
C38	3-*n*-Butylphathlide	10.013	$C_{12}H_{14}O_2$
C59	Levistilide A	9.377	$C_{24}H_{28}O_4$
C34	Senkyunolide A	0.864	$C_{12}H_{16}O_2$
C23	Carvone	0.803	$C_{10}H_{14}O$
C25	Saikosaponin A	0.593	$C_{42}H_{68}O_{13}$
C64	Oleanolic acid	0.56	$C_{30}H_{48}O_3$
C49	9-(acetyloxy)-8,8-dimethyl-2-oxo-9,10-dihydro-2H,8H-pyrano [2,3-f]chromen-10-yl 2-methyl-2-butenoate	0.542	$C_{21}H_{22}O_7$
C45	3-Butylidenephthalide	0.502	$C_{12}H_{12}O_2$
C24	Scoparone	0.385	$C_{11}H_{10}O_4$
C39	4-methyl-6-phenyl-5,6-dihydro-2H-pyran-2-one	0.372	$C_{12}H_{12}O_2$
C35	α-Pinene-2-oxide	0.269	$C_{10}H_{16}O$
C48	Gardenin B	0.237	$C_{19}H_{18}O_7$
C30	Methyl cinnamate	0.199	$C_{10}H_{10}O_2$
C1	DL-Arginine	0.19	$C_6H_{14}N_4O_2$
C9	Ferulic acid	0.142	$C_{10}H_{10}O_4$

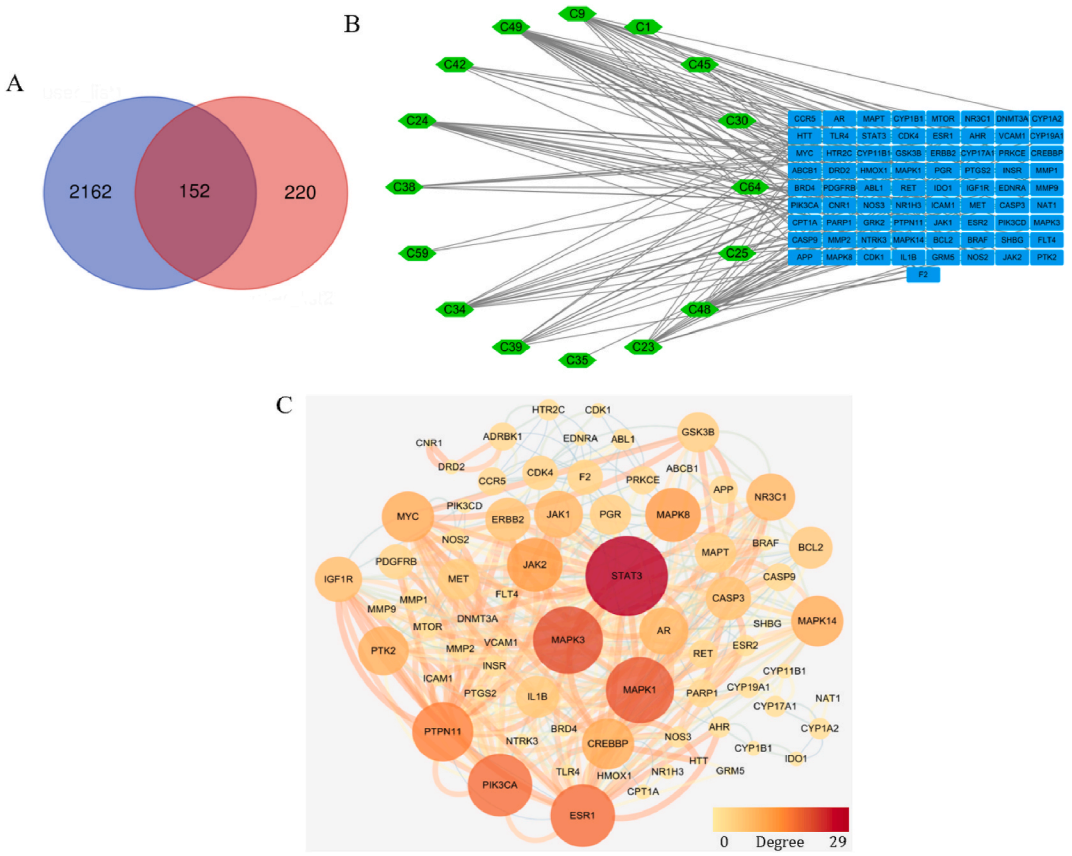

Fig. 2. Component-target analysis and protein-protein interaction analysis results of PEFC obtained using network pharmacology methods. (A) Venn diagram of overlapping targets between compound and depression–related targets. Component-related targets are indicated in red and disease-related targets are indicated in blue (B) compound-target network of PEFC against depression. (C) Protein-protein interaction (PPI) analysis network diagram of PEFC. The darker color and larger area of the nodes represents the greater the degree value, which means stronger the correlation with PEFC for depression.

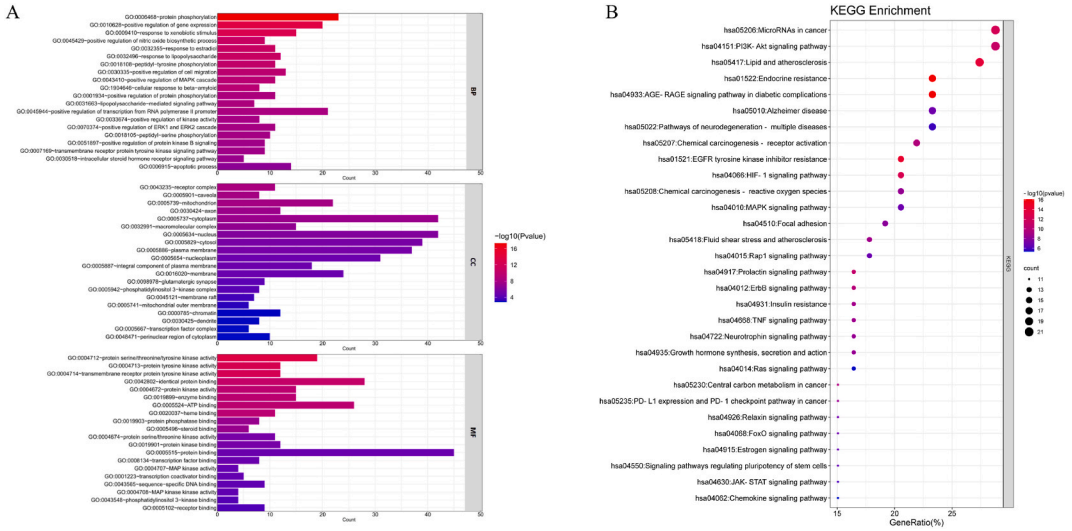

Fig. 3. GO and KEGG enrichment analyses of 73 targets for PEFC against depression. (A) Histogram of the top 20 terms in GO enrichment analysis. BP, biological process; CC, cellular component; MF, molecular function. (B) Bubble chart of top 30 signaling pathways in KEGG enrichment analysis.

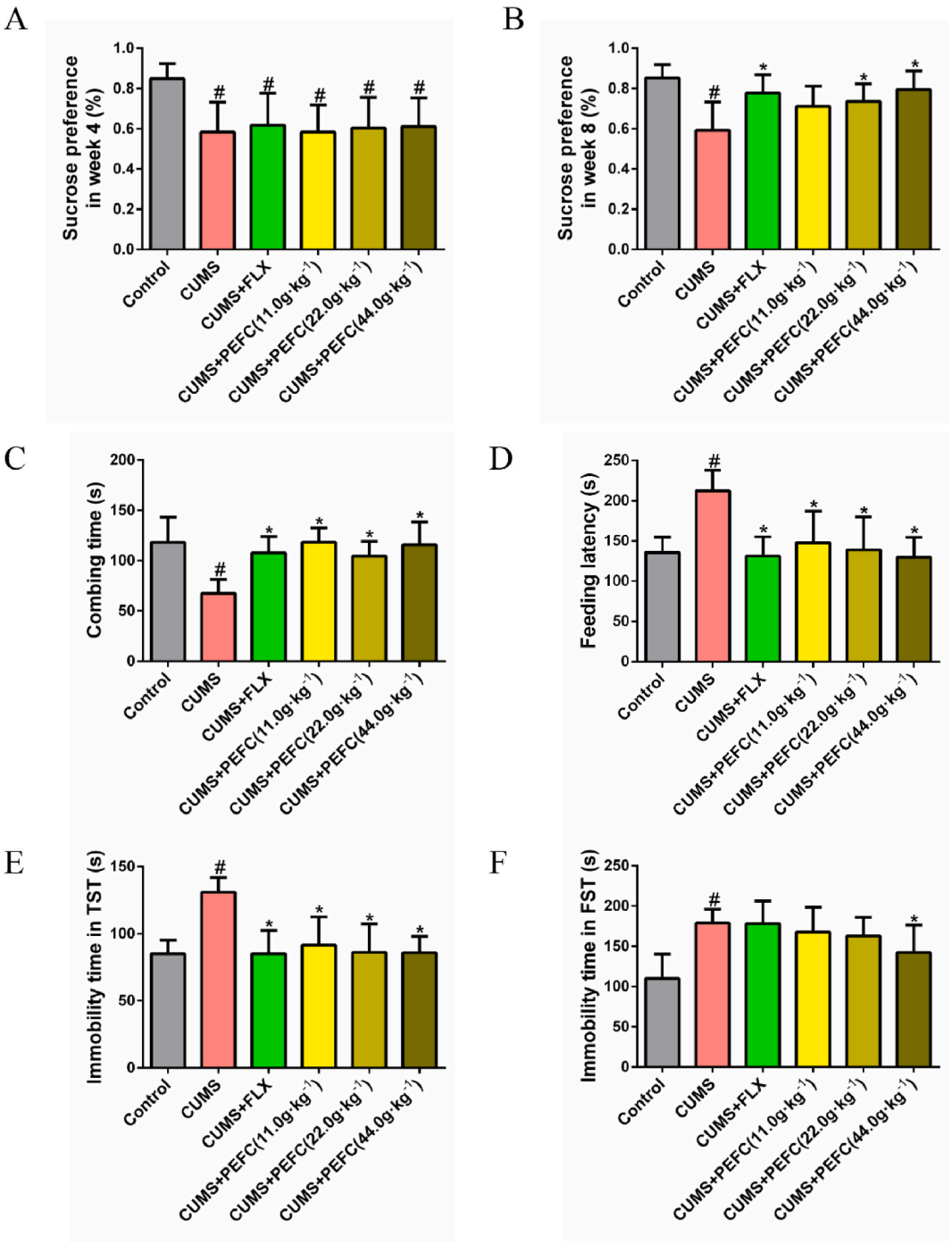

Fig. 4. PEFC ameliorates CUMS induced depression like behaviors in mice. (A) Sucrose preference test (SPT) at the end of the fourth week, (n = 10). (B) SPT after four weeks of administration (end of eighth week) (n = 10). (C) Combing time in the splash test (ST, n = 10). (D) Feeding latency in novelty suppressed feeding test (NFST, n = 10). (E) Immobility time in the tail suspension test (TST, n = 10). (F) Immobility time in the forced swimming test (FST, n = 10). Data were normalized to the control and presented as means ± SEM. $^{\#}P < 0.05$, *vs*. control; $^{*}P < 0.05$ *vs*. CUMS.

control animals ($P < 0.05$), reflecting the poorer self-care and apathetic behavior exhibited in depression. Mice given PEFC (11.0 g kg^{-1}, 22.0 g kg^{-1}, 44.0 g kg^{-1}, $P < 0.05$) or FLX ($P < 0.05$) for 4 weeks had substantially increased combing time compared to mice in the CUMS group (Fig. 4C). The NSFT revealed that mice in the CUMS group had a significantly longer feeding latency time than mice in the control groups ($P < 0.05$). This suggests that the CUMS process caused anxiety, which in turn led to a decreased desire for food in an unfamiliar setting. Treatment with PEFC (11.0 g kg^{-1}, 22.0 g kg^{-1}, 44.0 g kg^{-1}, $P < 0.05$) or FLX ($P < 0.05$) for four weeks significantly

decreased the model animals' eating latency (Fig. 4D).

Desperate behaviors in mice in the TST are measured by recording their immobility for a specific period. In the TST and FST, CUMS group remained immobile for significantly longer than those in the control group. ($P < 0.05$). In the TST, either one of PEFC (11.0 g kg^{-1}, 22.0 g kg^{-1}, 44.0 g kg^{-1}, $P < 0.05$) or FLX ($P < 0.05$) pointedly reduced the immobility time of the model animals (Fig. 4E). However, in the FST, only high doses of PEFC (44.0 g kg^{-1}, $P < 0.05$) glaringly downregulated FST immobility time (Fig. 4F). The lack of efficacy of FLX in FST is possibly associated with the reported adverse effects of the continuous administration of fluoxetine that cause cognitive and motor impairment manifestations [2]. These findings imply that PEFC can considerably reduce the depressive-like behaviors brought on by CUMS.

3.5. PEFC attenuated CUMS-induced Cort-GR dysfunction in mice

Hyperactivation of the HPA axis is the principal neuroendocrine change in depression and is primarily reflected by a significant increase in serum Cort. Serum Cort levels were substantially elevated in CUMS mice, and GR levels were significantly reduced in the mouse hippocampus compared with the control ($P < 0.01$). However, the administration of PEFC resulted in a drastic decline in serum Cort levels in model mice in a dose-dependent manner (11.0 g kg^{-1}, $P < 0.05$; 22.0 g kg^{-1}, $P < 0.01$; 44.0 g kg^{-1}, $P < 0.01$) (Fig. 5A) with a significant increase in hippocampal GR levels (22.0 g kg^{-1}, $P < 0.05$; 44.0 g kg^{-1}, $P < 0.01$); FLX had a similar modulatory effect ($P < 0.01$) (Fig. 5B and C).

3.6. PEFC improves the metabolic profiles of CUMS mice

To understand the metabolic role of PEFC in the CUMS model and to more intuitively predict its potential targets for antidepressant action, this research examined and analyzed differential metabolites in mouse hippocampal sample. Unsupervised PCA was used to scrutinize the data quality of metabolomics analysis, with the PCA scores showing complete separation of the CUMS model group from the control group (Fig. 6A), indicating that CUMS caused a disruption in the metabolic profiles of the mouse hippocampus. There were also significant changes in the hippocampal metabolic profiles of mice after FLX or PEFC treatment (Fig. 6B). Supervised analysis techniques, orthogonal partial least squares discriminant analysis (OPLS-DA), were utilized to maximize differences and screen for differential metabolites that led to class separation. All groups in the OPLS-DA model satisfied the 95% Hotelling T-squared distribution and showed primary partition ($R^2X = 0.748$; $R^2Y = 0.993$; $Q^2 = 0.654$) (Fig. 6C). The model demonstrated strong prediction, according to a 200-permutation cross-validation test used to evaluate statistical significance and predictive accuracy (Fig. 6D).

Metabolites meeting $P < 0.05$, FDR <0.05, and VIP >1.0 were retained as metabolites with massive differences on the online tool Biodeep Cloud Platform. The changes in metabolites induced by CUMS and FLX or PEFC treatments are shown in Table 3 and Fig. 7. According to these findings, the levels of a total of 44 metabolites were drastically changed in the CUMS group compared with the control group: four metabolites (including Vanillylmandelic acid, 3,4-Dihydroxyphenylpropanoate, and 2-Ketobutyric acid) were elevated, and 40 metabolites (including L-Proline, L-Asparagine, and L-Glutamine) were reduced. Remarkably, PEFC markedly restored the levels of metabolites including, L-Proline, L-Asparagine and L-Glutamine in CUMS mice. Furthermore, the metabolic pathways analysis was conducted to understand the underlying molecular functions of these hippocampal metabolite biomarkers. The potential biomarkers were found to be primarily involved in 61 disturbed metabolic pathways. Fig. 8 displays the metabolic pathway analysis of

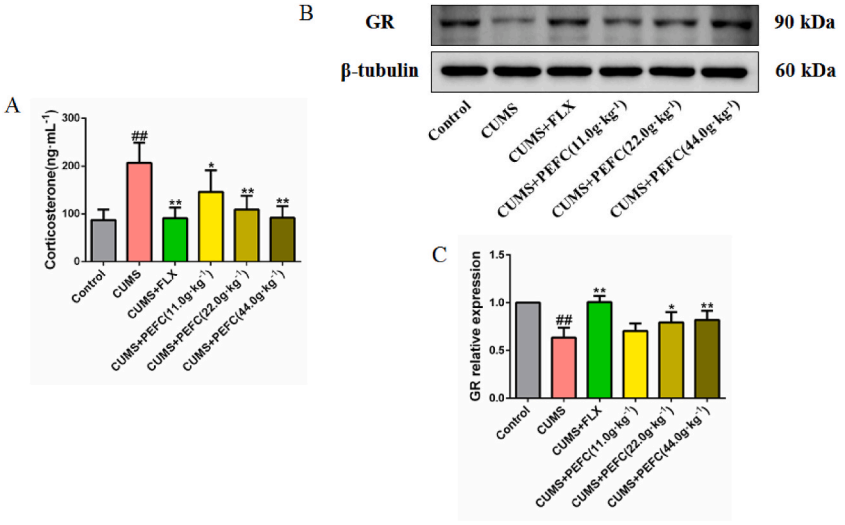

Fig. 5. Effect of PEFC on serum Cort levels and GR expression in the hippocampus of CUMS mice. (A) Serum levels of CORT in CUMS mice, n = 6 per group. (B) Representative Western Blot bands graphs and (C) statistical graphs of hippocampal GR protein expression levels in CUMS mice. Data were normalized to the control and presented as means ± SEM. $^{\#\#}P < 0.01$, *vs.* control; $^{*}P < 0.05$, $^{**}P < 0.01$ *vs.* CUMS.

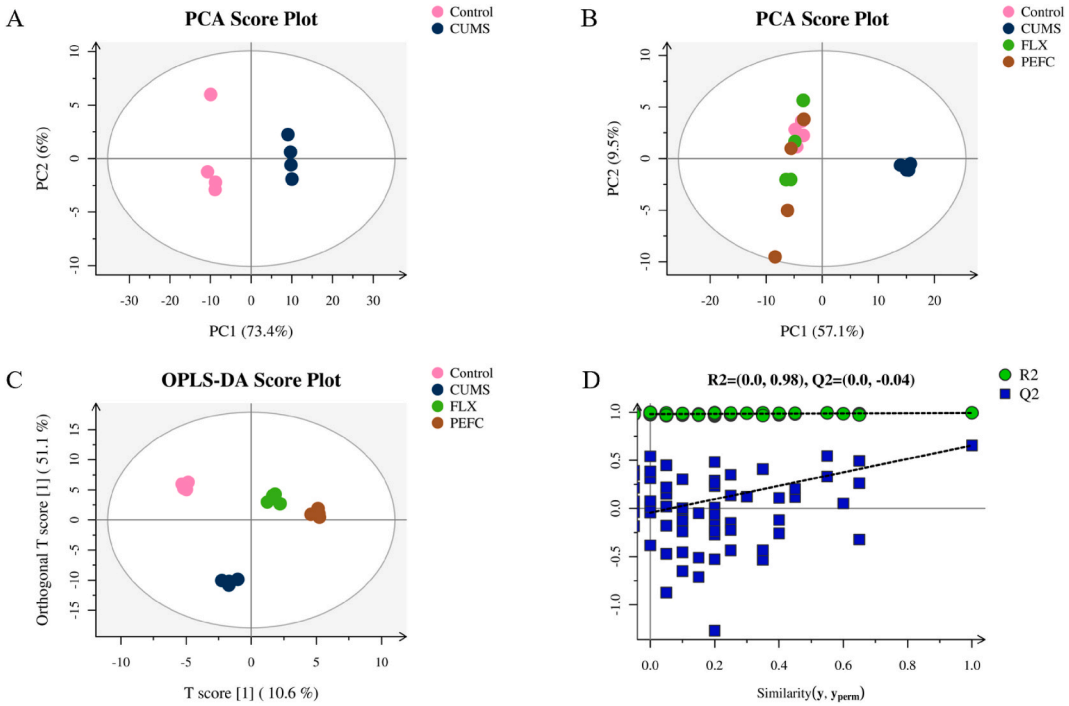

Fig. 6. Score plot of PCA (n = 4 per group) and multivariate statistical analysis of metabolic characteristics of mouse hippocampal samples. (A) PCA score chart of control group and the CUMS group. (B) Score plot of PCA between different animal groups. (C) Score plot of OPLS-DA between different animal groups. (D) Results of cross-validation between different animal groups.

these metabolites that experienced considerable alteration. These results suggest that amino acid biosynthesis, lysine degradation, glycine, serine and threonine metabolism, catecholamine inhibition, as well as the mTOR signaling pathway contribute to antidepressant effects of PEFC in CUMS mice.

3.7. Integrated analysis of network pharmacology and metabolomics

Based on network pharmacology and metabolomics, an interaction network was established to provide an integrated view of the processes by which PEFC combats depression. MetScape provides a bioinformatics framework for the visualization and interpretation of metabolomic and expression profiling data in the context of metabolism. It allows users to build and analyze networks of genes and metabolites [38]. The 44 differential metabolites resulting from metabolomics analysis were imported into Metscape, and "compound-gene" was selected as the network type and then the network was constructed to obtain 158 target genes associated with the differential metabolites. 158 target genes obtained by differential metabolites using the Metscope tool intersect with the 73 differential genes obtained in network pharmacology, 17 of them overlapped in the Venn diagram analysis (Fig. 9A; Supplementary Material, Table S6). The String database combined with Cytoscape was adopted for protein-protein interaction (PPI) network analysis of the intersecting targets, as shown in Fig. 9B. Targets, including *MTOR*, *MYC*, and *PIK3CA*, exert essential impacts on the antidepressant effects of PEFC. Fig. 9C and D show the top 10 key terms in GO functional enrichment and the top 10 critical KEGG pathways, respectively. KEGG analysis suggested that the ErbB signaling pathway and PI3K/Akt signaling pathway exhibited a relatively high number of target connections.

3.8. Validation of the PEFC antidepressant mechanism through the PI3K/Akt/mTOR signaling pathway

Metabolomics and KEGG analysis indicated that regulation of PI3K/Akt signaling pathway and mTOR are critical for PEFC to exert antidepressant effects. As shown in Fig. 9E, the panel displays the PI3K/Akt signaling pathway from the KEGG result. The red rectangle nodes stand for the most prominent genes associated with PEFC pharmacological actions. Western blot analysis (Fig. 10A) showed that p-PI3K/PI3K ($P < 0.05$), *p*-Akt/Akt ($P < 0.01$) and, *p*-mTOR/mTOR protein expression levels in the CUMS mouse model declined dramatically compared to the control group, and the phosphorylation levels of PI3K, AKT and mTOR were significantly higher after PEFC (44.0 g kg^{-1}) treatment (Fig. 10B–D). These results demonstrated that the antidepressant effects of PEFC were associated with the activation of the PI3K/AKT/mTOR signaling cascade.

Table 3
Significantly changed metabolites between different groups. The change of metabolites in the CUMS group compared to the control group, and the trend of improvement of metabolic profiles by drug treatment.

No.	Metabolites	p. value	-log10 (p)	FDR	vip	Trends in CUMS vs. control	Trends in treatment vs. CUMS
M1	Cycloheximide	0.0048	2.3144	0.0490	1.345	down	up
M2	Benzaldehyde	0.0067	2.1718	0.0490	1.756	down	up
M3	L-Proline	0.0067	2.1718	0.0490	1.876	down	up
M4	Phenylethylamine	0.0083	2.0785	0.0490	1.344	down	up
M5	L-Allothreonine	0.0084	2.074	0.0490	1.546	down	up
M6	L-Asparagine	0.0091	2.0385	0.0490	1.192	down	up
M7	Pipecolic acid	0.0091	2.0385	0.0490	1.657	down	up
M8	Spermidine	0.0091	2.0385	0.0490	1.818	down	up
M9	12-Hydroxydodecanoic acid	0.0097	2.012	0.0490	1.177	down	up
M10	8-Amino-7-oxononanoate	0.0101	1.9942	0.0490	1.766	down	up
M11	Azelaic acid	0.0101	1.9942	0.0490	1.761	down	up
M12	3,4-Dihydroxyphenylpropanoate	0.0106	1.9721	0.0490	1.365	up	down
M13	Guanidinosuccinic acid	0.0106	1.9721	0.0490	1.365	down	up
M14	Phenylacetic acid	0.0106	1.9721	0.0490	1.187	down	up
M15	6-Hydroxynicotinate	0.0121	1.9147	0.0490	1.715	down	up
M16	Pyridoxamine	0.0121	1.9147	0.0490	1.582	down	up
M17	Uracil	0.0121	1.9147	0.0490	1.684	down	up
M18	Oxoadipic acid	0.0125	1.9014	0.0490	1.068	down	up
M19	Polygodial	0.0132	1.8794	0.0490	1.36	down	up
M20	D-Ribose	0.0136	1.8661	0.0490	1.732	down	up
M21	Vanillylmandelic acid	0.0149	1.8265	0.0490	1.242	up	down
M22	5-Guanidino-3-methyl-2-oxopentanoate	0.0173	1.7605	0.0490	1.591	down	up
M23	Phenyl acetate	0.0173	1.7605	0.0490	1.461	down	up
M24	Erucic acid	0.0175	1.7561	0.0490	1.706	down	up
M25	2,3-Butanediol	0.0178	1.7474	0.0490	1.604	down	up
M26	Phosphorylcholine	0.0190	1.721	0.0490	1.261	down	up
M27	L-Methionine	0.0195	1.7079	0.0490	1.692	down	up
M28	Ascorbate	0.0197	1.7035	0.0490	1.575	down	up
M29	gamma-Aminobutyric acid	0.0197	1.7035	0.0490	1.21	down	up
M30	Piperidine	0.0227	1.6423	0.0490	1.282	down	up
M31	3,4-Dihydroxymandelic acid	0.0230	1.6379	0.0490	1.005	down	up
M32	Aminoadipic acid	0.0257	1.5899	0.0490	1.221	down	up
M33	Cytosine	0.0259	1.5855	0.0490	1.297	down	up
M34	Stearic acid	0.0259	1.5855	0.0490	1.068	up	down
M35	Inosine	0.0273	1.5637	0.0490	1.323	down	up
M36	L-Glutamine	0.0289	1.5376	0.0490	1.039	down	up
M37	21-Deoxycortisol	0.0307	1.5115	0.0490	1.209	down	up
M38	Niacinamide	0.0308	1.5115	0.0490	1.243	down	up
M39	L-Homoserine	0.0317	1.4985	0.0490	1.403	down	up
M40	1,2,3-Trihydroxybenzene	0.0321	1.4942	0.0490	1.227	down	up
M41	Taurine	0.034	1.4681	0.049495	1.37	down	up
M42	2-Ketobutyric acid	0.0391	1.4076	0.0536	1.337	up	down
M43	L-Rhamnofuranose	0.0454	1.3429	0.0405	1.11	down	up
M44	Maltol	0.0454	1.3429	0.0405	1.246	down	up

4. Discussion

Because of the complex pathogenesis of depression and the unclear changes in molecular and cellular signaling pathways, the current classical antidepressant treatments rarely have satisfactory efficacy, can cause severe side effects, and brought a heavy burden to the medical system. As a result, TCM has received much attention in the prevention and treatment of depression due to its multi-component, multi-target, multi-pathway, and low toxicity advantages [39]. Among them, the antidepressant effect of Xiaoyaosan has been demonstrated extensively [4,5]. CDB, as a streamlined formulation of Xiaoyaosan, has been verified to exert antidepressant effects comparable to those of Xiaoyaosan in different animal models [14,15]. However, the material basis of its antidepressant effect and potential mechanisms have not been fully identified, which limited the development as a new antidepressant herbal formula. Here, we obtained PEFC and characterized it by using UPLC-QE/MS. According to the findings, 73 components in all were detected from PEFC, 16 active compounds of which were further obtained via SwissADME screening. Among, Ligustilide, 3-*n*-butylphthalide, Levistilide A (from *Angelicae sinensis* (Oliv) Diels.); Carvone (from *Menthae haplocalyx* Briq.); and Saikosaponin A (from *Bupleurum scorzonerifolium* Willd.) were the most prevalent active compounds in PEFC, accounting for more than 80% of all detected peaks. Reportedly, Ligustilide could effectively attenuate CUMS-induced depression-like behavior in rats, and the possible mechanism was associated with higher levels of progesterone and allopregnanolone in the prefrontal cortex and hippocampus [40]. 3-*n*-butylphthalide has been found to exhibit antidepressant effects by activating the BDNF/ERK/mTOR cascade in the cortex of CUMS rat model, thereby enhancing synaptic protein synthesis [41]. Carvone, one of the significant components of coriander volatile oil, allegedly showed

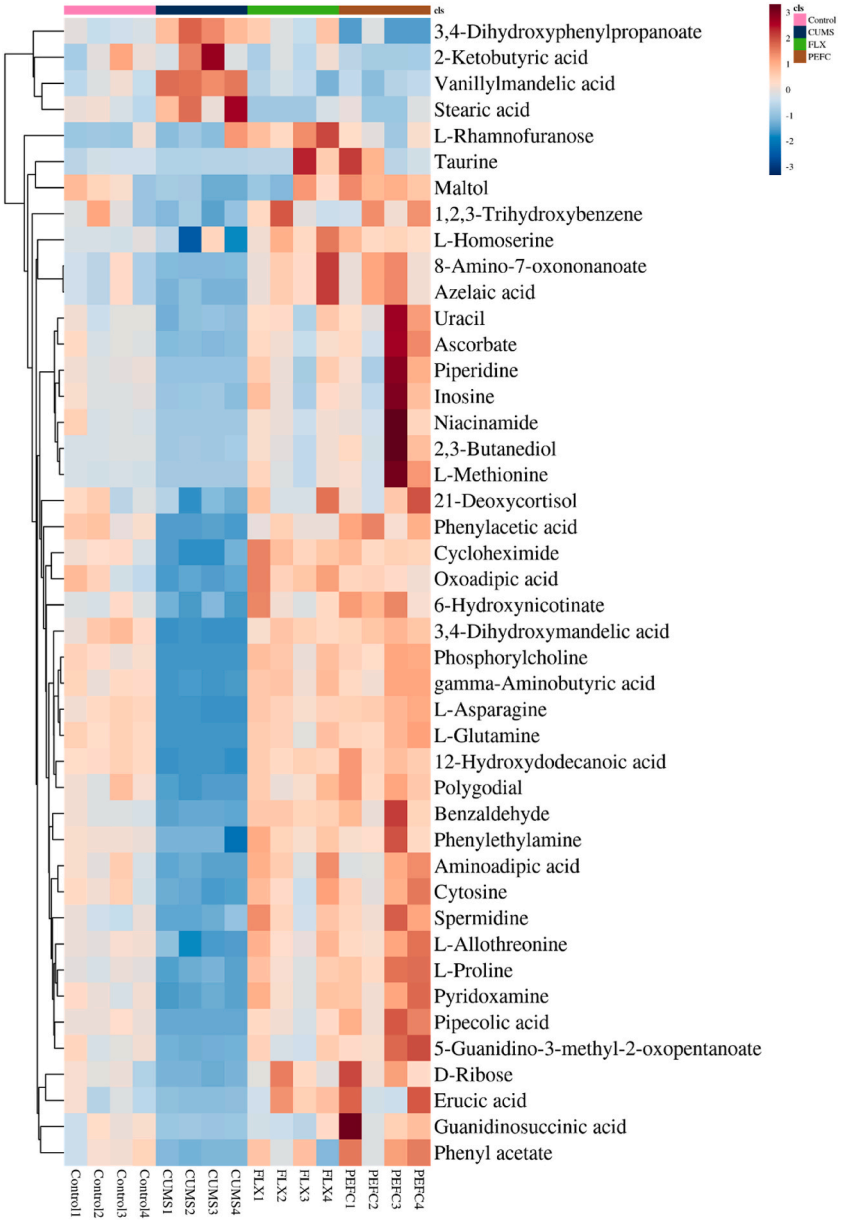

Fig. 7. Differentiation of differential metabolites in control, CUMS, FLX and PEFC (44.0 g kg^{-1}) groups. p value < 0.05, FDR < 0.05 and VIP value > 1.0, n $= 4$ per group.

antidepressant properties in a rat model of Alzheimer's disease with β-amyloid (1–42) [42]. Reports also verified that Saikosaponin A significantly improves depression-like behaviors in multiple depressed animal models, and its antidepressant mechanisms include the activation of the CREB/BDNF pathway in the hippocampal DG region to inhibit hippocampal neuronal apoptosis [43], the upregulation of proline-rich transmembrane protein 2 (PRRT2) expression to increase hippocampal dopamine content [44], and the inhibition of the HPA axis hyperactivation to reduce hippocampal neuroinflammation [45]. These findings suggested that these compounds are the material basis for the antidepressant effect of PEFC and explain its multi-targeted action characteristics.

Depression is directly linked to stress in both its onset and progression. The CUMS technique is one of the most widely used mouse chronic stress models in recent research because it replicates the ongoing annoyance that people experience in reaction to uncontrollably negative social experiences [3]. CUMS resulted in mice showing a series of typical depression-like features such as reducing sucrose preference, prolonging TST/FST immobility, extending feeding latency, and shortening grooming time in mice. According to our findings, CUMS-induced depression-like traits in mice were significantly alleviated after four weeks of treatment with PEFC. This suggests that PEFC possesses antidepressant qualities comparable to those of FLX. The over-activation of the HPA axis is a widely recognized marker for the diagnosis and therapy of depression [46]. An imbalance in the feedback regulation of the HPA axis results in

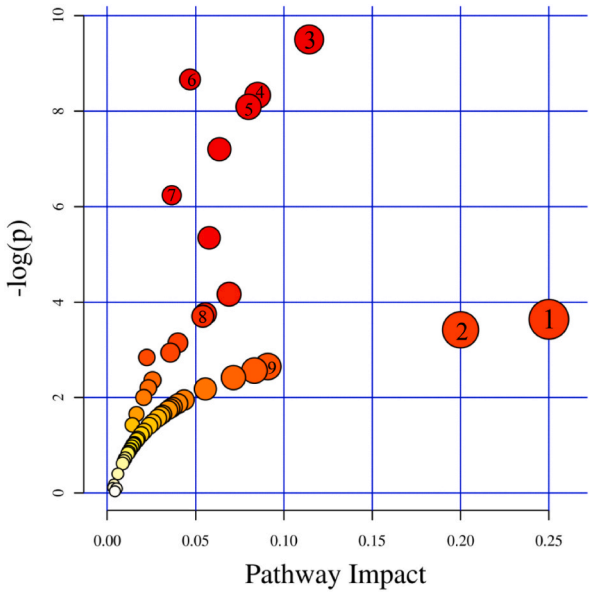

Fig. 8. Metabolic pathways involved in the treatment of PEFC on CUMS mice. (1) Catecholamine transferase inhibitors; (2) Lysine degradation; (3) Biosynthesis of amino acids; (4) Glycine, serine and threonine metabolism; (5) Cysteine and methionine metabolism; (6) Protein digestion and absorption; (7) Aminoacyl-tRNA biosynthesis; (8) mTOR signaling pathway; (9) Cholinergic synapse.

elevated levels of cortisol peripherally and centrally. The glucocorticoid receptor (GR) is a crucial component of the negative feedback regulation of the HPA axis specifically for Cort [47]. In this study, CUMS mice exhibited a rise in serum Cort level and a significant reduction in GR expression in the hippocampus, showing functional abnormalities of CORT-GR. This status was reversed by PEFC treatment, which reflected that the antidepressant effects of PEFC are partially consistent with the predicted role of the *NR3C1* gene and the action on the endocrine resistance mechanism predicted in the network pharmacology analysis.

Network pharmacology analysis revealing that *STAT3*, *MAPK1/3*, *PIK3CA*, *ESR1*, *JAK2*, *NR3C1* and other subjects as the potential antidepressant targets of PEFC. GO and KEGG enrichment analysis further found PEFC might be exert its antidepressant effects through regulating the PI3K-Akt signaling pathway, endocrine resistance, the MAPK signaling pathway, the neurotrophy signaling pathway and the JAK-STAT3 signaling pathway. Evidence suggests that *STAT3* was a key coordinator of cytokine activation in cellular immune responses [48,49], stress can trigger the phosphorylation of the JAK2/STAT3 signaling pathway, leading to abnormal microglia activation, which further upregulated the level of cytokines, exacerbating neuroinflammation in depression [50]. Additionally, *MAPK1/3* genes encode ERK2 and ERK1 on the MAPK signaling pathway, which play essential roles in neuronal and glial cell proliferation/differentiation and synaptic plasticity [51]. The neuroendocrine pathway in which the hormones are involved is also a major underlying mechanism of depression: *ESR1* encode the estrogen receptor 1, and estrogen is implicated in the neuroprotective activity and regulation of neuronal activity is crucial to understanding the etiology of mood disorders [52]. These results predict that PEFC might be able to influence multiple genes/proteins in the development of depression, whereby reflecting the multi-target, multi--pathway characteristics of PEFC as an antidepressant.

After receiving PEFC therapy, the levels of 44 metabolites in the CUMS group showed significant changes in the LC-MS-based non-targeted hippocampus metabolomic study. Amino acids are well known to be involved in the pathophysiological mechanisms of depression [53]. Glutamate (Glu) is synthesized from glutamine (Gln) by glutaminase (GS) in neurons and then released into the synaptic gap to exert neuroexcitatory effects [54]. Glu is also metabolized to γ-aminobutyric acid (GABA) by glutamic acid decarboxylase (GAD). The Gln-Glu-GABA cycle is critical to excitatory and inhibitory neurotransmission as part of glial-neuronal communication and has significant implications for depressive processes [55]. Studies using the CUMS model have shown that Gln is reduced in both the plasma and brain of depressed mice, a possible indicator for the objective evaluation of depression [56]. High levels of CORT suppress Gln levels, resulting in poor neural viability and inadequate excitatory neurotransmission; enhancing Gln provides promising clues for the treatment of depression [57]. In another research, in a systematic analysis of the metabolomic changes in animal models of depression employing vote counting statistics (VCS), γ-aminobutyric acid, although acting as an inhibitory neurotransmitter, was more downregulated in the hippocampal region ($VCS = -10$, $p = 0.038$) [58]. In the present investigation, glutamine and γ-aminobutyric acid levels were decreased in the hippocampus. L-proline is a structural homolog of GABA, and its accumulation in GABAergic neurons can competitively inhibit glutamate decarboxylase, leading to reduced GABA production and impairing synaptic plasticity [59]. Asparagine has a sedative effect under conditions of biological central stress and is associated with neurological defects during embryonic development [60]. Reduced levels of serum asparagine or proline have been reported in Wistar Kyoto (WKY) rats (a model rat for depression) and in patients with depressed mood and can be reversed by antidepressant treatment in both scenarios [61,62], consistent with our findings. Glycine is a non-essential amino acid that can be converted to serine under certain conditions and plays a crucial role in metabolic regulation and neurological function [63]. Glycine- or serine-conjugated glutamate

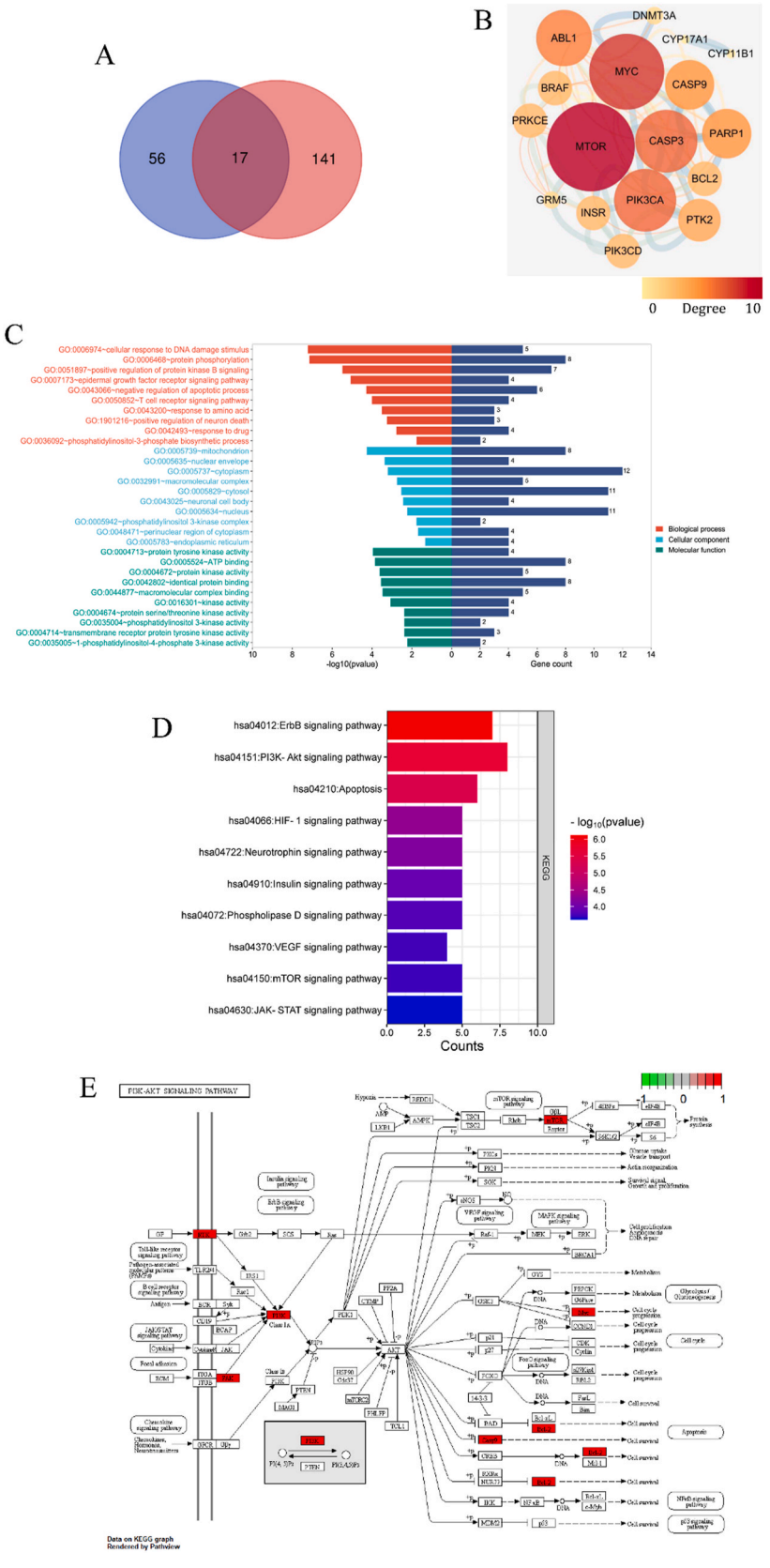

(caption on next page)

Fig. 9. Combined network pharmacology and metabolomics to analyze the target of PEFC in depression. (A) The Venn analysis showed the crosstalk of PEFC in two omics, (metabolomics in red and network pharmacology in blue); (B) PPI network of intersection targets; (C) The GO enrichment analysis of intersection targets; (D) Top 10 significantly enriched pathways enrichment by KEGG analysis; (E) KEGG pathway suggested that various targets in PI3K/Akt signaling were tightly associated with PEFC pharmacological action. The red rectangle nodes represent the most significant genes or biological pathways associated with PEFC pharmacological action.

acts as a co-antagonist to help activate N-methyl-D-aspartate receptors (NMDARs), and the abnormal activity of NMDARs has been demonstrated to reduce neuroplasticity, leading to emotional and cognitive impairment [64,65]. A recent study on serum metabolomic analysis in depression patients revealed that the dysregulation of glycine and serine metabolism can lead to depressive and anxiety symptoms [66]. The main biological functions of L-methionine include methylation (transmethylation) of various molecules and synthesis of cysteine, and eventually serine, regulating the production of endogenous polysulfides, which may exert neuroprotective effects through glutathione production [67,68]. Previous reports found that plasma levels of the related sulfide Thiocystine in depressed patients regressed after treatment with Xiaoyaosan, suggesting that Xiaoyaosan may exert antidepressant effects by regulating cysteine and methionine metabolism [69]. In our current investigation, consistent with the mechanism of action of most documented antidepressants, PEFC upregulated the levels of glutamine, γ-aminobutyric acid, asparagine, and proline in the hippocampus of CUMS mice and regulated the metabolism of glycine, serine, and threonine.

In the ensuing integrated analysis of network pharmacology and metabolomics, targets such as *PIK3CA*, *MTOR*, *MYC*, and the PI3K/Akt/mTOR signaling pathways were highlighted. *PIK3CA* encodes the p110 catalytic subunit of PI3K, as an important intracellular kinase is involved in the PI3K/Akt signaling pathway, one of the most active signaling pathway for intercellular communication, which regulated cell differentiation, metabolism, several growth factors, and cytoskeletal reorganization, leading to neuronal survival and apoptosis [8,70]. The maturation of stem cells and brain progenitor cells at the synaptic level is intimately associated with PI3K activity during development [71]. Additionally, reduced brain volume accompanying behavioral deficits in Akt gene-deficient mice, suggested a key role for Akt in depression [72]. mTOR integrates a range of extracellular signals crucial in protein synthesis and neuroplasticity, making it a key effector protein downstream of PI3K/Akt [73]. The activation of mTOR pathway accelerates the cell cycle interphase of neural precursor cells, thus rapidly tracking the proliferation and differentiation of neurons, and mTOR further increases the expression of long-temporal enhancement (LTP)-related proteins, which play a positive role in neuroplasticity [74]. Furthermore, the inhibition of mTOR has been achieved in clinical [75,76] and animal studies. Cumulative reports indicated that the activation of mTOR is the basis of antidepressant effects of a variety of natural products [77]. More importantly, the activation of mTOR signaling is required for the rapid antidepressant effects of NNMDA antagonists (e.g. ketamine) and could be a potential target for the development of fast-acting antidepressants [78]. In the present study, Western blot of mouse hippocampal samples was used to

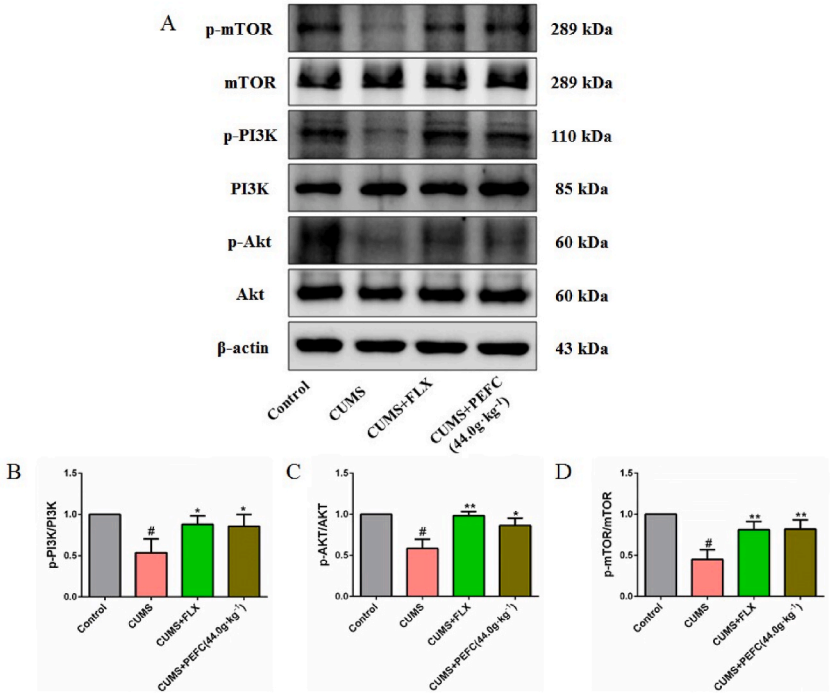

Fig. 10. PEFC alleviated the Inhibition of the PI3K/Akt signaling pathway in the hippocampus of CUMS mice. (A) Representative protein bands of PI3K/Akt/mTOR signaling pathway (PI3K, p-PI3K, AKT, *p*-AKT, mTOR, *p*-mTOR) in the hippocampus of mice. Statistical graphs of relative protein expression of ratio of p-PI3K/PI3K (B), ratio of *p*-AKT/AKT (C) and ratio of *p*-mTOR/mTOR (D). Data were normalized to the control and presented as means ± SEM. $^{\#}P < 0.05$, *vs.* control; $^{*}P < 0.05$, $^{**}P < 0.01$ *vs.* CUMS.

validate the prediction of the combined network pharmacology and metabolomics analysis. Consistent with previous studies [79,80], CUMS inhibits PI3K/Akt/mTOR signalling in the hippocampus and PEFC reverses this impairment, which implies that PI3K/Akt/mTOR signaling was a target of PEFC antidepressants.

5. Conclusion

In conclusion, the current work used a thorough approach integrating metabolomics to examine potential PEFC processes in the treatment of depression, network pharmacology and molecular biology experiments. Our results indicate that PEFC attenuates CUMS-induced depression-like behavior mainly associated with activation of PI3K/Akt/mTOR pathways, which is at least partially responsible for the improvement of depression by PEFC. This study confirmed the antidepressant effectiveness of PEFC and elucidated more specific mechanisms, which may provide solid evidence for the mechanistic exploration and preclinical application of PEFC.

Funding statement

This work was supported by the Applied Basic Research Project of Science and Technology Department of Sichuan Province (20YYJC0640), the Open Research Fund of Chengdu University of Traditional Chinese Medicine Key Laboratory of Systematic Research of Distinctive Chinese Medicine Resources in Southwest China (2020XSGG002), and the Xinglin Scholar Research Promotion Project of Chengdu University of Traditional Chinese Medicine (CDTD2018014, QNXZ2018022), Chengdu Medical Research Project (2019039).

Data availability statement

The datasets used and/or analyzed during the current study are available from the corresponding author upon reasonable request.

Ethical approval

All processes involving mice were authorized by the Chengdu University of Traditional Chinese Medicine College of Pharmacy's Committee for Animal Care and Use of Laboratory Animals approved the experimental procedures; TCM-2019-312 was the approval number for this process. Animal studies were performed in compliance with the ARRIVE guidelines. All animals received humane care according to the National Institutes of Health (USA) guidelines.

Additional information

The following supplementary materials can be seen in the submitted manuscript.

CRediT authorship contribution statement

Jiuseng Zeng: Writing – original draft, Data curation, Conceptualization. **Li Chen:** Supervision, Project administration, Data curation. **Xi Peng:** Validation, Software. **Fei Luan:** Investigation, Formal analysis. **Jingwen Hu:** Validation, Software. **Zhiqiang Xie:** Software. **Hongxiao Xie:** Validation. **Rong Liu:** Resources, Funding acquisition. **Haizhen Lv:** Supervision. **Nan Zeng:** Writing – review & editing, Supervision, Funding acquisition, Conceptualization.

Declaration of competing interest

The authors declare that they have no known competing financial interests or personal relationships that could have appeared to influence the work reported in this paper.

Abbreviations

Akt	protein kinase B
BDNF	brain derived neurotrophic factor
BP	biological process
CC	cellular component
CDB	Chaidangbo
Cort	corticosterone
CREB	cAMP-response element binding protein
CUMS	chronic unpredictable mild stress
ERK	extracellular regulated protein kinases
FLX	fluoxetine hydrochloride
FST	forced swimming test
GABA	γ-aminobutyric acid

Gln	glutamine
Glu	Glutamate
GO	Gene Ontology
HPLC	high-performance liquid chromatography
JAK	Janus kinase
JNK	c-Jun N-terminal kinase
KEGG	Kyoto Encyclopedia of Genes and Genomes
MAPK	mitogen-activated protein kinase
MF	molecular function
mTOR	mammalian target of rapamycin
NFST	novelty suppressed feeding test
NMDARs	N-methyl-D-aspartate receptors
OPLS-DA	orthogonal partial least squares discriminant analysis
PCA	principal component analysis
PEFC	petroleum ether fraction of CDB
PI3K	phosphatidylinositol 3-kinase
PPI	protein-protein interaction
SPT	sucrose preference test
ST	splash test
STAT3	Signal Transducer and Activator of Transcription 3
TCM	Traditional Chinese medicine
TST	tail suspension test

Appendix A. Supplementary data

Supplementary data to this article can be found online at https://doi.org/10.1016/j.heliyon.2024.e28582.

References

[1] S. Difrancesco, F. Lamers, H. Riese, K.R. Merikangas, A.T.F. Beekman, A.M. van Hemert, R.A. Schoevers, B. Penninx, Sleep, circadian rhythm, and physical activity patterns in depressive and anxiety disorders: a 2-week ambulatory assessment study, Depress. Anxiety 36 (2019) 975–986.

[2] A. Revet, F. Montastruc, A. Roussin, J.P. Raynaud, M. Lapeyre-Mestre, T.T.H. Nguyen, Antidepressants and movement disorders: a postmarketing study in the world pharmacovigilance database, BMC Psychiatr. 20 (2020) 308.

[3] J. Zeng, Y. Ji, F. Luan, J. Hu, Y. Rui, Y. Liu, Z. Rao, R. Liu, N. Zeng, Xiaoyaosan ethyl acetate fraction alleviates depression-like behaviors in CUMS mice by promoting hippocampal neurogenesis via modulating the IGF-1Rβ/PI3K/Akt signaling pathway, J. Ethnopharmacol. 288 (2022) 115005.

[4] X. Liu, C. Liu, J. Tian, X. Gao, K. Li, G. Du, X. Qin, Plasma metabolomics of depressed patients and treatment with Xiaoyaosan based on mass spectrometry technique, J. Ethnopharmacol. 246 (2020) 112219.

[5] X.M. Zhou, C.Y. Liu, Y.Y. Liu, Q.Y. Ma, X. Zhao, Y.M. Jiang, X.J. Li, J.X. Chen, Xiaoyaosan alleviates hippocampal glutamate-induced toxicity in the CUMS rats via NR2B and PI3K/Akt signaling pathway, Front. Pharmacol. 12 (2021) 586788.

[6] J. Chen, C. Lei, X. Li, Q. Wu, C. Liu, Q. Ma, J. Chen, Research progress on classical traditional Chinese medicine formula xiaoyaosan in the treatment of depression, Front. Pharmacol. 13 (2022) 925514.

[7] C. Chen, Q. Yin, J. Tian, X. Gao, X. Qin, G. Du, Y. Zhou, Studies on the potential link between antidepressant effect of Xiaoyao San and its pharmacological activity of hepatoprotection based on multi-platform metabolomics, J. Ethnopharmacol. 249 (2020) 112432.

[8] M. He, Z.Q. Wu, C.T. Que, J.B. Zou, T. Zhang, S.Q. Yang, F. Wang, X. Wang, N. Zeng, Study on the antidepressant effects and mechanisms of composition drug-group of Xiaoyao Powder, Chin. Med. Pharmaco Clin. 30 (2014) 5–9.

[9] X. Wang, Q. Feng, Y. Xiao, P. Li, Radix Bupleuri ameliorates depression by increasing nerve growth factor and brain-derived neurotrophic factor, Int. J. Clin. Exp. Med. 8 (2015) 9205–9217.

[10] Y. Feng, X. Gao, M. Meng, H. Xue, X. Qin, Multi-omics reveals the mechanisms of antidepressant-like effects of the low polarity fraction of Bupleuri Radix, J. Ethnopharmacol. 256 (2020) 112806.

[11] W. Gong, Y. Zhou, X. Li, X. Qin, G. Du, Research progress in antidepressive active ingredients and pharmacological effects of Angelicae Sinensis Radix, Chin. Tradit. Herb. Drugs 47 (2016) 3905–3911.

[12] Y. Liu, H. Li, S. Wu, L. Wang, Antidepressant effects of water extracts from Angellica sinensis (Oliv) Diels, mice. Pharmacol. Clin. Chin. Mater. Med. 33 (2017) 106–109.

[13] J. Xue, H. Li, X. Deng, Z. Ma, Q. Fu, S. Ma, L-Menthone confers antidepressant-like effects in an unpredictable chronic mild stress mouse model via NLRP3 inflammasome-mediated inflammatory cytokines and central neurotransmitters, Pharmacol. Biochem. Behav. 134 (2015) 42–48.

[14] X. He, X. Wang, B. Shi, J. Luo, X. Liu, X. Peng, N. Zeng, R. Liu, Study on BDNF pathways molecular mechanisms for the antidepressant effects of composition drug-group of Xiaoyaosan in CUMS rats, Pharm Clin Chin Mat Med 10 (2019) 18–22.

[15] X. Wang, R. Liu, J. Luo, X. Liu, B. Shi, X. Ye, N. Zeng, Study on the antidepressant effects and mechanisms via BDNF/HPA of composition drug-group of Xiaoyao Powder based on CUMS rats, Chin. Med. Pharmaco Clin. 34 (2018) 14–19.

[16] Y. Li, X. Yang, S. Chen, L. Wu, J. Zhou, K. Jia, W. Ju, Integrated network pharmacology and GC-MS-based metabolomics to investigate the effect of Xiang-Su volatile oil against Menopausal depression, Front. Pharmacol. 12 (2021) 765638.

[17] A.D. Flores, W.S. Yu, M.L. Fung, L.W. Lim, Neuromodulation and hippocampal neurogenesis in depression: a scoping review, Brain Res. Bull. 188 (2022) 92–107.

[18] C. Geng, Y. Guo, C. Wang, D. Liao, W. Han, J. Zhang, P. Jiang, Systematic impacts of chronic unpredictable mild stress on metabolomics in rats, Sci. Rep. 10 (2020) 700.

[19] R. Magalhães, A. Novais, D.A. Barrière, P. Marques, F. Marques, J.C. Sousa, J.J. Cerqueira, A. Cachia, T.M. Jay, M. Bottlaender, N. Sousa, S. Mériaux, F. Boumezbeur, A Resting-state functional MR imaging and spectroscopy study of the dorsal Hippocampus in the chronic unpredictable stress rat model, J. Neurosci. 39 (2019) 3640–3650.

[20] X. Zhou, J. Wang, Y. Lu, C. Chen, Y. Hu, P. Liu, X. Dong, Anti-depressive effects of Kai-Xin-San on lipid metabolism in depressed patients and CUMS rats using metabolomic analysis, J. Ethnopharmacol. 252 (2020) 112615.
[21] A. Di Minno, M. Gelzo, M. Stornaiuolo, M. Ruoppolo, G. Castaldo, The evolving landscape of untargeted metabolomics, Nutr Metab Cardiovasc Dis 31 (2021) 1645–1652.
[22] M. Danhof, Systems pharmacology - towards the modeling of network interactions, Eur. J. Pharmaceut. Sci. 94 (2016) 4–14.
[23] N. Yuan, L. Gong, K. Tang, L. He, W. Hao, X. Li, Q. Ma, J. Chen, An integrated pharmacology-based analysis for antidepressant mechanism of Chinese herbal formula Xiao-Yao-San, Front. Pharmacol. 11 (2020) 284.
[24] H.Q. Wang, H.T. Liu, L. Wang, L. Min, B. Chen, H. Li, Uncovering the active components, prospective targets, and molecular mechanism of Baihe Zhimu decoction for treating depression using network pharmacology-based analysis, J. Ethnopharmacol. 281 (2021) 114586.
[25] S.Y. Qu, X.Y. Li, X. Heng, Y.Y. Qi, P.Y. Ge, S.J. Ni, Z.Y. Yao, R. Guo, N.Y. Yang, Y. Cao, Q.C. Zhang, H.X. Zhu, Analysis of antidepressant activity of huang-Lian Jie-Du decoction through network pharmacology and metabolomics, Front. Pharmacol. 12 (2021) 619288.
[26] R. Zhang, X. Zhu, H. Bai, K. Ning, Network pharmacology databases for traditional Chinese medicine: review and assessment, Front. Pharmacol. 10 (2019) 123.
[27] D. Zhang, Y. Zhang, Y. Gao, X. Chai, R. Pi, G. Chan, Y. Hu, Translating traditional herbal formulas into modern drugs: a network-based analysis of Xiaoyao decoction, Chin. Med. 15 (2020) 25.
[28] A. Daina, V. Zoete, Application of the SwissDrugDesign online resources in virtual screening, Int. J. Mol. Sci. 20 (2019) 4612.
[29] M. Chu, T. Gao, X. Zhang, W. Kang, Y. Feng, Z. Cai, P. Wu, Elucidation of potential targets of san-Miao-San in the treatment of Osteoarthritis based on network pharmacology and molecular docking analysis, Evid Based Complement Alternat Med 2022 (2022) 7663212.
[30] W. Huang da, B.T. Sherman, R.A. Lempicki, Systematic and integrative analysis of large gene lists using DAVID bioinformatics resources, Nat. Protoc. 4 (2009) 44–57.
[31] S. Antoniuk, M. Bijata, E. Ponimaskin, J. Wlodarczyk, Chronic unpredictable mild stress for modeling depression in rodents: meta-analysis of model reliability, Neurosci. Biobehav. Rev. 99 (2019) 101–116.
[32] B. Shi, J. Luo, Y. Fang, X. Liu, Z. Rao, R. Liu, N. Zeng, Xiaoyao Pills prevent lipopolysaccharide-induced depression by inhibiting inflammation and protecting nerves, Front. Pharmacol. 10 (2019) 1324.
[33] M.F. Ferreira, L. Castanheira, A.M. Sebastião, D. Telles-Correia, Depression assessment in clinical trials and pre-clinical tests: a critical review, Curr. Top. Med. Chem. 18 (2018) 1677–1703.
[34] S.S. Valvassori, G.C. Dal-Pont, R.B. Varela, W.R. Resende, F.F. Gava, F.G. Mina, J. Budni, J. Quevedo, Ouabain induces memory impairment and alter the BDNF signaling pathway in an animal model of bipolar disorder: cognitive and neurochemical alterations in BD model, J. Affect. Disord. 282 (2021) 1195–1202.
[35] M.J. Ramaker, S.C. Dulawa, Identifying fast-onset antidepressants using rodent models, Mol. Psychiatr. 22 (2017) 656–665.
[36] C.A. Vadnie, L.M. DePoy, C.A. McClung, Measuring the effects of circadian rhythm-related manipulations on depression-like behavior in rodents: forced swim and tail suspension tests, Methods Mol. Biol. 2130 (2021) 69–78.
[37] G. Unal, R. Canbeyli, Psychomotor retardation in depression: a critical measure of the forced swim test, Behav. Brain Res. 372 (2019) 112047.
[38] W. Xu, B. Hu, Y. Cheng, Y. Guo, W. Yao, H. Qian, Material basis research for Echinacea purpurea (L.) Moench against hepatocellular carcinoma in a mouse model through integration of metabonomics and molecular docking, Phytomedicine 98 (2022) 153948.
[39] C. Bi, S. Guo, S. Hu, J. Chen, M. Ye, Z. Liu, The microbiota-gut-brain axis and its modulation in the therapy of depression: comparison of efficacy of conventional drugs and traditional Chinese medicine approaches, Pharmacol. Res. 183 (2022) 106372.
[40] J.C. Ma, H.L. Zhang, H.P. Huang, Z.L. Ma, S.F. Chen, Z.K. Qiu, J.S. Chen, Antidepressant-like effects of Z-ligustilide on chronic unpredictable mild stress-induced depression in rats, Exp. Ther. Med. 22 (2021) 677.
[41] C. Chen, H. Ma, Z. Fu, Antidepressant-like effect of 3-n-Butylphthalide in rats exposed to chronic unpredictable mild stress: modulation of brain-derived neurotrophic factor level and mTOR activation in cortex, Neurochem. Res. 46 (2021) 3075–3084.
[42] O. Cioanca, L. Hritcu, M. Mihasan, A. Trifan, M. Hancianu, Inhalation of coriander volatile oil increased anxiolytic-antidepressant-like behaviors and decreased oxidative status in beta-amyloid (1-42) rat model of Alzheimer's disease, Physiol. Behav. 131 (2014) 68–74.
[43] A.R. Wang, L.F. Mi, Z.L. Zhang, M.Z. Hu, Z.Y. Zhao, B. Liu, Y.B. Li, S. Zheng, Saikosaponin A improved depression-like behavior and inhibited hippocampal neuronal apoptosis after cerebral ischemia through p-CREB/BDNF pathway, Behav. Brain Res. 403 (2021) 113138.
[44] J. Guo, F. Zhang, J. Gao, X. Guan, B. Liu, X. Wang, Z. Qin, K. Tang, S. Liu, Proteomics-based screening of the target proteins associated with antidepressant-like effect and mechanism of Saikosaponin A, J. Cell Mol. Med. 24 (2020) 174–188.
[45] X.Q. Chen, S.J. Chen, W.N. Liang, M. Wang, C.F. Li, S.S. Wang, S.Q. Dong, L.T. Yi, C.D. Li, Saikosaponin A attenuates perimenopausal depression-like symptoms by chronic unpredictable mild stress, Neurosci. Lett. 662 (2018) 283–289.
[46] Y. Chai, Q. Li, Y. Wang, E. Tao, T. Asakawa, The value of HPA Axis hormones as biomarkers for screening and early diagnosis of postpartum depression: updated information about methodology, Front. Endocrinol. 13 (2022) 916611.
[47] F. Zhao, W. Tao, Z. Shang, W. Zhang, J. Ruan, C. Zhang, L. Zhou, H. Aiello, H. Lai, R. Qu, Facilitating granule cell survival and maturation in dentate gyrus with baicalin for antidepressant therapeutics, Front. Pharmacol. 11 (2020) 556845.
[48] D. Enache, C.M. Pariante, V. Mondelli, Markers of central inflammation in major depressive disorder: a systematic review and meta-analysis of studies examining cerebrospinal fluid, positron emission tomography and post-mortem brain tissue, Brain Behav. Immun. 81 (2019) 24–40.
[49] A.S. Shariq, E. Brietzke, J.D. Rosenblat, Z. Pan, C. Rong, R.M. Ragguett, C. Park, R.S. McIntyre, Therapeutic potential of JAK/STAT pathway modulation in mood disorders, Rev. Neurosci. 30 (2018) 1–7.
[50] Z. Qu, N. Zheng, Y. Wei, Y. Chen, Y. Zhang, M. Zhang, H. Chang, J. Liu, H. Ai, X. Geng, Q. Wang, L. Yin, Effect of cornel iridoid glycoside on microglia activation through suppression of the JAK/STAT signalling pathway, J. Neuroimmunol. 330 (2019) 96–107.
[51] J.Q. Wang, L. Mao, The ERK pathway: molecular mechanisms and treatment of depression, Mol. Neurobiol. 56 (2019) 6197–6205.
[52] M.E. Talarowska, J. Szemraj, S. Kuan-Pin, Expression of ESR1 and ESR2 oestrogen receptor encoding gene and personality traits - preliminary study, Prz Menopauzalny 18 (2019) 133–140.
[53] H. Chen, H. Xie, S. Huang, T. Xiao, Z. Wang, X. Ni, S. Deng, H. Lu, J. Hu, L. Li, Y. Wen, D. Shang, Development of mass spectrometry-based relatively quantitative targeted method for amino acids and neurotransmitters: applications in the diagnosis of major depression, J. Pharm. Biomed. Anal. 194 (2021) 113773.
[54] A. Egerton, A.A. Grace, J. Stone, M.G. Bossong, M. Sand, P. McGuire, Glutamate in schizophrenia: neurodevelopmental perspectives and drug development, Schizophr. Res. 223 (2020) 59–70.
[55] L.E. Ramos-Languren, A. Avila-Luna, G. García-Díaz, R. Rodríguez-Labrada, Y. Vázquez-Mojena, C. Parra-Cid, S. Montes, A. Bueno-Nava, R. González-Piña, Glutamate, glutamine, GABA and oxidative products in the pons following cortical injury and their role in motor functional recovery, Neurochem. Res. 46 (2021) 3179–3189.
[56] Y.P. Chen, C. Wang, J.P. Xu, Chronic unpredictable mild stress induced depression-like behaviours and glutamate-glutamine cycling dysfunctions in both blood and brain of mice, Pharm. Biol. 57 (2019) 280–286.
[57] S.F. Chu, Z. Zhang, X. Zhou, W.B. He, B. Yang, L.Y. Cui, H.Y. He, Z.Z. Wang, N.H. Chen, Low corticosterone levels attenuate late life depression and enhance glutamatergic neurotransmission in female rats, Acta Pharmacol. Sin. 42 (2021) 848–860.
[58] J. Pu, Y. Liu, S. Gui, L. Tian, Y. Yu, X. Song, X. Zhong, X. Chen, W. Chen, P. Zheng, H. Zhang, X. Gong, L. Liu, J. Wu, H. Wang, P. Xie, Metabolomic changes in animal models of depression: a systematic analysis, Mol. Psychiatr. 26 (2021) 7328–7336.
[59] G.W. Crabtree, A.J. Park, J.A. Gordon, J.A. Gogos, Cytosolic accumulation of L-proline disrupts GABA-ergic transmission through GAD blockade, Cell Rep. 17 (2016) 570–582.
[60] C.L. Lomelino, J.T. Andring, R. McKenna, M.S. Kilberg, Asparagine synthetase: function, structure, and role in disease, J. Biol. Chem. 292 (2017) 19952–19958.
[61] M. Nagasawa, T. Otsuka, S. Yasuo, M. Furuse, Chronic imipramine treatment differentially alters the brain and plasma amino acid metabolism in Wistar and Wistar Kyoto rats, Eur. J. Pharmacol. 762 (2015) 127–135.

[62] J. Peplinska-Miaskowska, H. Wichowicz, R. Smoleński, P. Jablonska, L. Kaska, The comparison of nucleotide metabolites and amino acids patterns in patients with eating disorders, with and without symptoms of depression, Nucleos Nucleot. Nucleic Acids 41 (2022) 333–341.
[63] M. Imenshahidi, H. Hossenzadeh, Effects of glycine on metabolic syndrome components: a review, J. Endocrinol. Invest. 45 (2022) 927–939.
[64] B. Peyrovian, J.D. Rosenblat, Z. Pan, M. Iacobucci, E. Brietzke, R.S. McIntyre, The glycine site of NMDA receptors: a target for cognitive enhancement in psychiatric disorders, Prog. Neuro-Psychopharmacol. Biol. Psychiatry 92 (2019) 387–404.
[65] L. Curcio, M.V. Podda, L. Leone, R. Piacentini, A. Mastrodonato, P. Cappelletti, S. Sacchi, L. Pollegioni, C. Grassi, M. D'Ascenzo, Reduced D-serine levels in the nucleus accumbens of cocaine-treated rats hinder the induction of NMDA receptor-dependent synaptic plasticity, Brain 136 (2013) 1216–1230.
[66] Y. Du, J. Wei, Z. Zhang, X. Yang, M. Wang, Y. Wang, X. Qi, L. Zhao, Y. Tian, W. Guo, Q. Wang, W. Deng, M. Li, D. Lin, T. Li, X. Ma, Plasma metabolomics profiling of metabolic pathways affected by major depressive disorder, Front. Psychiatr. 12 (2021) 644555.
[67] H. Kimura, Physiological role of hydrogen sulfide and polysulfide in the central nervous system, Neurochem. Int. 63 (2013) 492–497.
[68] J. Lin, M. Akiyama, I. Bica, F.T. Long, C.F. Henderson, R.N. Goddu, V. Suarez, B. Baker, T. Ida, Y. Shinkai, P. Nagy, T. Akaike, J.M. Fukuto, Y. Kumagai, The uptake and release of polysulfur cysteine species by cells: physiological and toxicological implications, Chem. Res. Toxicol. 32 (2019) 447–455.
[69] C. Liu, Plasma Metabolomics Studies on the Clinical Antidepressant Effect of Xiaoyaosan, Shanxi University, 2016. Thesis for Master degree.
[70] Q. Zhan, Y. Wu, L. Liu, Effects of notoginsenoside R1 on attenuating depressive behavior induced by chronic stress in rats through induction of PI3K/AKT/NF-κB pathway, Drug Dev. Res. 83 (2022) 97–104.
[71] A. Brandmaier, S.Q. Hou, W.H. Shen, Cell cycle control by PTEN, J. Mol. Biol. 429 (2017) 2265–2277.
[72] A.M. Tsimberidou, A. Skliris, A. Valentine, J. Shaw, U. Hering, H.H. Vo, T.O. Chan, R.S. Armen, J.R. Cottrell, J.Q. Pan, P.N. Tsichlis, AKT inhibition in the central nervous system induces signaling defects resulting in psychiatric symptomatology, Cell Biosci. 12 (2022) 56.
[73] M. Fujiki, K.M. Yee, O. Steward, Non-invasive high frequency repetitive transcranial magnetic stimulation (hfrTMS) robustly activates molecular pathways implicated in neuronal growth and synaptic plasticity in select populations of neurons, Front. Neurosci. 14 (2020) 558.
[74] S. Maity, M. Chandanathil, R.M. Millis, S.A. Connor, Norepinephrine stabilizes translation-dependent, homosynaptic long-term potentiation through mechanisms requiring the cAMP sensor Epac, mTOR and MAPK, Eur. J. Neurosci. 52 (2020) 3679–3688.
[75] C.S. Jernigan, D.B. Goswami, M.C. Austin, A.H. Iyo, A. Chandran, C.A. Stockmeier, B. Karolewicz, The mTOR signaling pathway in the prefrontal cortex is compromised in major depressive disorder, Prog. Neuro-Psychopharmacol. Biol. Psychiatry 35 (2011) 1774–1779.
[76] L.A. Averill, C.L. Averill, R. Gueorguieva, S. Fouda, M. Sherif, K.H. Ahn, M. Ranganathan, D.C. D'Souza, S.M. Southwick, G. Sanacora, R.S. Duman, J.H. Krystal, C.G. Abdallah, mTORC1 inhibitor effects on rapid ketamine-induced reductions in suicidal ideation in patients with treatment-resistant depression, J. Affect. Disord. 303 (2022) 91–97.
[77] C. Lu, X. Liu, J. Li, Y. Huang, X. Huang, G. Dai, L. Wu, Merazin hydrate produces rapid antidepressant effects depending on activating mTOR signaling by upregulating downstream synaptic proteins in the Hippocampus, ACS Chem. Neurosci. 12 (2021) 3939–3946.
[78] P. Zanos, T.D. Gould, Mechanisms of ketamine action as an antidepressant, Mol. Psychiatr. 23 (2018) 801–811.
[79] J.X. Zhu, J.L. Shan, W.Q. Hu, J.X. Zeng, J.C. Shu, Gallic acid activates hippocampal BDNF-Akt-mTOR signaling in chronic mild stress, Metab. Brain Dis. 34 (2019) 93–101.
[80] M. Xu, F. Xiao, M. Wang, T. Yan, H. Yang, B. Wu, K. Bi, Y. Jia, Schisantherin B improves the pathological manifestations of mice caused by behavior desperation in different ages-depression with cognitive impairment, Biomol Ther (Seoul). 27 (2019) 160–167.